Modeling and optimization of hydrogenation of CO_2

Available online at www.sciencedirect.com

ScienceDirect

journal homepage: www.elsevier.com/locate/he

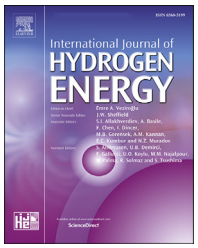

Modeling and optimization of hydrogenation of CO_2: Estimation of kinetic parameters via Artificial Bee Colony (ABC) and Differential Evolution (DE) algorithms

Sara Najari [a], *Gyula Gróf* [b], *Samrand Saeidi* [b,*], *Fausto Gallucci* [c]

[a] *Department of Chemical Engineering, Tarbiat Modares University, Tehran 14115-114, Iran*
[b] *Department of Energy Engineering, Budapest University of Technology and Economics, Budapest, Hungary*
[c] *Inorganic Membranes and Membrane Reactors, Eindhoven University of Technology, Department of Chemical Engineering and Chemistry, Eindhoven, The Netherlands*

ARTICLE INFO

Article history:
Received 24 September 2018
Received in revised form
1 January 2019
Accepted 3 January 2019
Available online 1 February 2019

Keywords:
CO_2 hydrogenation
RWGS
FT
Optimization
ABC algorithm
DE algorithm

ABSTRACT

Global warming, climate change, fossil fuel depletion and steep hikes in the price of environmentally friendly hydrocarbons motivate researchers to investigate CO_2 hydrogenation for hydrocarbons production. However, due to the reaction complexities and varieties of produced species, the process mechanism and subsequently estimation of the kinetic parameters have been controversial yet. Therefore, estimating the kinetic parameters using Artificial Bee Colony (ABC) and Differential Evolution (DE) optimization algorithms based on Langmuir-Hinshelwood-Hougen-Watson (LHHW) mechanism is proposed as a possible remedy to fulfil the requirements. To this end, a one-dimensional heterogeneous model comprising detailed reaction rates of reverse water gas shift (RWGS), Fisher-Tropsch (FT) reactions and direct hydrogenation (DH) of CO_2 is developed. It is observed that ABC exhibiting 6.3% error in predicting total hydrocarbons selectivity is superior to DE algorithm with 32.9% error. Therefore, the model employed the estimated kinetic parameters obtained via ABC algorithm, is exploited for products distribution analysis. Results reveal that maximum 73.21% hydrocarbons (C_1–C_4) selectivity can be achieved at 573 K and 1 MPa with 0.85% error compared to the experimental value of 72.59%. Accordingly, the proposed model can be exploited as a powerful tool for evaluating and predicting the performance of CO_2 hydrogenation to hydrocarbons process.

Introduction

Growing global energy consumption has enhanced anthropogenic CO_2 emissions, which has driven research towards solutions to mitigate CO_2 emissions. In addition to optimize energy utilization processes as well as enhancing the energy conversion efficiency (e.g., in power plants), one of the potential strategies for reducing CO_2 emissions would be CO_2 hydrogenation to produce methanol and fuels [1–4].

* *Corresponding author.*
E-mail address: samrand@energia.bme.hu (S. Saeidi).
https://doi.org/10.1016/j.ijhydene.2019.01.020

Fortunately, hydrogen can be obtained from various sources including fossil fuels (steam reforming, catalytic partial oxidation, auto thermal reforming), water splitting (electrolysis, thermolysis and photo-reduction) and biomass gasification [5–10]. However, considering challenging issues of conventional energy sources, clean and affordable energy systems are required to be developed [11,12]. In this regards, sustainable and renewable sources comprising geothermal, wind, solar, and ocean attracted extensive attention as emerging technologies of hydrogen production [13–15]. Recently, hydrogenation of CO_2 to value added products has attracted great attention as an emerging technology. Therefore, hydrogenation has been considered as a potential technology to produce value-added products via simultaneous occurrence of CO_2 shift and FT reactions [16].

Previous investigations have shown that CO_2 hydrogenation begins with a two-step mechanism [17–20]. The first step includes conversion of CO_2 to CO according to the RWGS reaction Eq. (1):

$$CO_2 + H_2 \leftrightarrow CO + H_2O \quad \Delta H_{573\,K} = +38\ kJ/mol \tag{1}$$

Afterwards, the produced CO from RWGS involves in the FT reaction for hydrocarbons production according to Eq. (2):

$$nCO + 2nH_2 \rightarrow (CH_2)_n + nH_2O \quad \Delta H_{573\,K} = -166\ kJ/mol \tag{2}$$

The transient behavior using both CO/H_2 and CO_2/H_2 was almost identical, including a series of reactions; however, CO_2 activation requires much longer time. The products distribution at steady state condition was almost the same using both gas mixtures, implying that hydrocarbons formation from CO_2 improves while CO is a transient product [16].

It was proposed by Fiato et al. [21] that the DH of CO_2 contributes to hydrocarbons could be possible by applying iron carbide catalysts (Eq. (3)). Moreover, this reaction is suggested to be improved through CO_2 dissociative adsorption on catalyst active site (*) followed by the hydrogenation of adsorbed carbon species. In order to synthesize the long chain hydrocarbons, H_2/CO_2 ratio should be 3. As shown in Table 1, if H_2/CO_2 ratio is adjusted to 4 the reaction will proceed towards methane formation through the Sabatier process [22,23].

$$nCO_2 + 3nH_2 - \rightarrow (CH_2)_n + 2nH_2O \quad \Delta H_{573\,K} = -128\ kJ/mol \tag{3}$$

Regarding the kinetics of the CO_2 shift reaction, various literature studies are reported. Compared to the water gas shift reaction (WGS), CO_2 shift reaction or RWGS occurs faster in the presence of various oxides and metallic catalysts while exhibiting lower activation energy (see Table 2) [24].

Up to the present, CO_2 hydrogenation has been investigated mostly over catalysts traditionally utilized for the FT reactions. The main product was methane when using Ni or Ru catalysts supported on silica [26]. Only a small amount of hydrocarbons with more than one carbon atom, were detected at the applied process conditions [19]. The influence of varying CO/CO_2 ratios using Co as an active metal on the synthesis gas were investigated in the previous research [27]. Increasing CO_2 content, resulted in methane formation as the most product instead of typical FT reactions which led mainly to hydrocarbons. Commonly, Co catalysts do not present great activity for both CO formation via RWGS reaction and hydrocarbon formation through FT reactions at moderate temperatures [28,29]. Thus, using such conditions, selective desorption of desired products after reversible CO adsorption which is a prerequisite on Co catalysts for long-chain hydrocarbons synthesis, is not possible [30–32].

Generally, Fe has shown the most favorable characteristics for the production of long-chain hydrocarbons through hydrogenation of CO_2 [33]. Fe which is known as a widely used metal for commercial hydrocarbons production via FT synthesis, is also utilized in CO shift reaction. Consequently, many efforts have been devoted to improve the catalytic properties of Fe-based catalysts through the use of various support materials or the addition of binder and promoters [18,34]. The most efficient Fe catalysts for CO_2 hydrogenation were obtained utilizing Al_2O_3 as support [35]. Meanwhile, potassium was applied as the promoter in concentrations of up to 0.5 mol K/mol of Fe [36]. Moreover, it was shown that SiO_2-coated Fe–K/γ-Al_2O_3 catalysts with different silica contents were prepared and examined for the synthesis of hydrocarbons from CO_2 hydrogenation. It was found that SiO_2 coating influenced both the activity for CO_2 conversion and the selectivity to higher hydrocarbons, depending on the loading level. The catalyst containing 9 wt% SiO_2 coating exhibited both high CO_2 conversion (63%) and high selectivity toward C_2^+ hydrocarbons (74%) [37].

As already reported, the efficiency of CO_2 hydrogenation is generally much lower than that of CO for production of long-chain hydrocarbons, due to low reactant conversion and high

Table 1 – Initial steps of hydrocarbon production with respect to the feed ratio (proposed by authors).

No	H_2/CO_2 ratio	Reactions
1		$Fe^{3+} + CO_2 + {}^* \rightarrow CO_2{}^*$
2	1	$H_2 + 2^* \rightarrow 2H^*$
3		$CO_2{}^* + H^* \rightarrow COOH^* + {}^*$
4		$COOH^* + H^* \rightarrow CO^* + {}^* + H_2O$
5	2	$H_2 + 2^* \rightarrow 2H^*$
6		$CO^* + H^* \rightarrow COH^* + {}^*$
7		$COH^* + H^* \rightarrow COH_2{}^* + {}^*$
8	3	$H_2 + 2^* \rightarrow 2H^*$
9		$COH_2{}^* + H^* \rightarrow CH_2{}^* + HO^*$
10		$HO^* + H^* \rightarrow H_2O$
		$CO_2 + 3\,H_2 \rightarrow CH_2{}^* + 2H_2O$
11	4	$H_2 + 2^* \rightarrow 2H^*$
12		$CH_2{}^* + H^* \rightarrow CH_3{}^* + {}^*$
13		$CH_3{}^* + H^* \rightarrow CH_4 + {}^* + Fe^{2+}$
		$CO_2 + 4\,H_2 \rightarrow CH_4 + 2H_2O$ (Sabatier reaction)

Table 2 – Reported values of apparent activation energies for CO_2 shift reaction.

Catalyst	E (kJ/mol)	T (K)	Ref.
FeSi–H	81	523–673	[25]
FeSi	56.72	523–673	[25]
FeSi–K	68.98	523–673	[25]
Fe_3O_4/Cr_2O_3	~80	600–700	[24]
Fe_3O_4	~80	600–700	[24]

CH_4 selectivity [16]. As Fe–K/γ-Al_2O_3 was recently reported to be remarkably active and efficient for CO_2 hydrogenation to long-chain hydrocarbons, this catalyst is chosen to be examined practically in this study [38]. However, a number of issues associated with the performance of this catalyst should be solved for the future commercial applications. Previous research has indicated the promising effects of binder addition to the catalyst [39]. Some binders are not only chemically active, especially at high temperatures, but also are somewhat catalytically active. In fact, interactions between the binder and catalysts have a strong effect on the activity and selectivity of the catalyst in CO_2 hydrogenation. The presence of binder in the catalyst can change the catalyst acidity. For example, the results of previous study showed that a ZSM-5 catalyst containing high amount of silica could improve the activity of acid catalyzed reactions through the formation of new acid sites during the catalyst fabrication owing to the zeolite-alumina interactions [40]. The acidity of the catalyst affects the CO_2 conversion and selectivity towards the hydrocarbons. It was reported that CO_2 conversion can be increased with the amount of medium acid sites while the selectivity to high-chain hydrocarbons was improved with increasing the amounts of strong acid sites [40]. Adding silica as a binder to the Fe–K/γ-Al_2O_3 catalyst causes a decrease in amounts of acid sites, and hence, a reduction in the acidity of the catalyst and iron-carbide (Fe–C). It is mentioned that the amount of Fe–C is associated with the catalyst activity (reactant conversion) whereas the strength of Fe–C determines the hydrocarbons chain length.

Thus, a few efforts have been made to model the CO_2 hydrogenation process in order to achieve a better understanding of the influential parameters. However, in all cases the FT reaction was just considered as a sole reaction for hydrocarbons production. For instance, Riedel et al. [27] proposed a scheme consisting three reactions of CO_2 shift, FT and DH and derived the corresponding kinetic parameters via regression. In a more recent study, Willauer et al. [41] included CO_2 methanation along with C_3H_6 formation, and determined the corresponding kinetic parameters via utilizing experimental results in the presence of Mn and K-promoted Fe catalysts supported on γ-alumina. Although there have been some studies on the significant issues regarding hydrogenation of CO_2 to hydrocarbons such as the effects of catalysts, operating conditions and reactor configurations, kinetics parameters as crucial factors of the corresponding reactions have not been sufficiently investigated.

One of the well-known optimization algorithms to estimate the kinetic parameters is the evolutionary algorithm compromising genetic algorithm (GA) and DE. For instance, Yan et al. [42], Chen et al. [43] and Hu et al. [44] employed chaos genetic algorithm, new clonal selection algorithm, hierarchical differential evolution and adaptive differential evolution to estimate kinetic parameters, respectively [45]. DE is an evolutionary algorithm that calculates the vector of differences between arbitrarily selected candidate solution vectors and employs these differences for the production of new, enhanced candidate solutions to develop its evolutionary search and optimization process. Although, DE is suitable for fine tuning and exploitations, but the risk of premature convergence because of its lack of explorations limited its utilization. In this regard, swarm intelligent (SI) algorithms such as particle swarm optimization (PSO), ABC, artificial fish swarm (AFS), and ant colony (AC) have attracted much attention for diverse optimization goals in the fields of engineering, science and mathematics. The ABC algorithm mimics the candidate solutions as a swarm of bees that forage through a search space for continuously better quality food sources (i.e., candidate solutions). However, none of the SI subordinates were utilized for the estimation of kinetic parameters so far. In addition, there is no research conducting comparison between two meta-heuristic algorithms like ABC and DE. Obviously, DE and ABC try to achieve the same goal (i.e., dynamic adaptation of the degrees of explorations and exploitations), but using different methodologies. However, ABC is more robust against premature convergence owing to its more explorative design (i.e., explicit explorations by employed and scout bees), in contrast to DE which exhibits premature convergence risk.

With regard to the lack of knowledge on the steps and details of CO_2 hydrogenation, effort has been made to estimate the kinetic parameters of this process for the first time through ABC and DE optimization algorithms based on LHHW mechanism. To this aim, both experimental and theoretical studies are accomplished. Firstly, CO_2 hydrogenation is performed in a lab-scale fixed-bed reactor containing synthesized Fe–K/γ-Al_2O_3 catalysts. In the next step, CO_2 hydrogenation process including RWGS, FT and DH reactions is simulated via a one-dimensional heterogeneous model. The next and the main part of this study is devoted to estimate the kinetic parameters of this process through ABC and DE optimization algorithms via utilization of the experimental results. Finally, based on the superiority of ABC algorithm to determine hydrocarbons distribution, the proposed model is exploited to investigate the reactor performance. Besides, available literature data are used to prove the validity of the modeling approach.

Experimental works

The main parts of the practical works, which are the catalyst preparation and reactor tests, are explained in this section. The results of the experiments are used for the estimation of kinetic parameters in the reaction rates and consequently determination of the reactant conversion and product distribution along the reactor length.

Catalyst preparation

In this study, impregnation method was used for catalyst preparation. The nominal catalyst compositions were calculated as 1.6Fe/0.4 K/8γ-Al_2O_3 on the basis of mass balance. Fe$(NO_3)_3 \cdot 9H_2O$ and K_2CO_3 were homogeneously mixed with small amount of water. Then, γ-Al_2O_3 particles were impregnated with aqueous solutions of metal salts and the solution was evaporated for 5 h at 358 K. Afterwards, the wet powder was dried at 383 K in the oven for 12 h followed by milling in the ball-mill for 1.5 h in order to reduce particle size to overcome intraparticle mass transfer limitations, even in the catalyst pores saturated with liquid hydrocarbons. Silica

binder (SiO_2), 3 wt% of the whole catalyst weight was added to the catalyst powder. Finally, the catalysts were mixed and dried at 383 K for 12 h followed by calcination at 773 K for 24 h (heating with 2 K/min to 773 K) in air. Brunauer-Emmett-Teller surface area was determined as 136 m^2/g for the dried catalyst, which provided a bed density of 1.00 g/cm^3.

Process description

A schematic diagram of the experimental rig is illustrated in Fig. 1. The reactor consists of an SS316 tube with the length of 60 cm and inner and outer diameters of 0.8 cm and 1.2 cm, respectively. In the typical experiments designed for kinetics rate derivation, a certain amounts of catalyst (1.5–5 gr) diluted with 60–100 mesh glass beads was prepared to fill the whole length of the reactor in order to achieve different space velocities. The dilution of the catalyst with inert substances such as glass beads can configure a uniform gas flow, and hence, prevents a high pressure drop along the catalyst bed while providing almost isothermal conditions through the catalyst bed. The temperature gradient along the catalyst bed was always between 2 and 5 K, depending on the applied reaction temperature. Flow rates of reactant gases (CO_2, H_2 and Ar) were controlled by mass flow controller (MFC, Brooks Co.). Reaction temperature was controlled within 563–633 K employing an electrical furnace and temperature control system. Reaction pressure was regulated by back pressure regulator and measured by pressure sensor. An ice-water cold trap was placed at the outlet of the reactor to condense out water from the product gas stream. Uncondensed gases (CO_2, CO, CH_4, H_2, C_2H_6, C_2H_4, C_3H_8, C_3H_6, n-C_4H_{10} and C_4H_8) were directed to a GC equipped with TCD (Carbosphere column) and FID (Poraplot-Q column) to be analyzed. The flow rates of the exit gases were measured with a wet gas meter.

Before each reaction test, the reactor was purged with Ar (flow rate 120 ml/min) at 593 K for 1 h followed by reduction of catalyst using H_2/Ar mixture flow (10% H_2 in Ar, 10 cm^3 of H_2 per min and per g of Fe in the catalyst, and holding time of 8 h). For reduction of the Fe catalyst, the two step reduction has been reported [46]. First, Fe_2O_3 is reduced to Fe_3O_4 and later reduced to metallic Fe, as shown in Eqs. (4) and (5):

$$3Fe_2O_3 + H_2 \rightarrow 2Fe_3O_4 + H_2O \quad (4)$$

$$Fe_3O_4 + 4H_2 \rightarrow 3Fe + 4H_2O \quad (5)$$

After reduction, the reactor temperature was adjusted to the desired temperature by furnace, the reaction pressure of 1 MPa, the desired H_2/CO_2 molar ratio and reactant flow rate were set to conduct CO_2 hydrogenation. When the steady state condition was reached, new reaction conditions were set. The reaction conditions in the experimental reactor (ER) are presented in Table 3.

According to the proposed reaction network at the first step, CO_2 is converted to CO through RWGS reaction, then CO reacts with H_2 through FT reactions at the second step and hydrocarbon products (C_2–C_4) are produced.

Mathematical modeling

The mathematical modeling of the reactor (Fig. 2) is carried out with the following assumptions:

Table 3 – Operating conditions of CO_2 hydrogenation to hydrocarbons.

Parameter	Value	Unit
H_2/CO_2 molar ratio	3	–
Feed gas temperature	563–633	K
Reactor pressure	1	MPa
GHSV	500–2000	$L/g_{cat}.h$

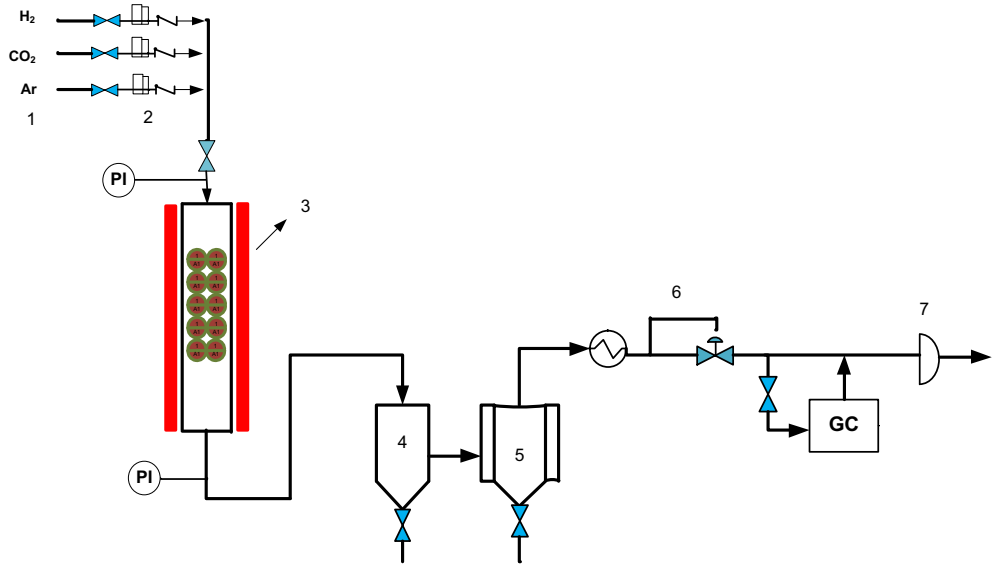

Fig. 1 – Experimental rig used for CO_2 hydrogenation to hydrocarbons, 1) Reactant gases (2) Mass flow controller, (3) Furnace, (4) G/L separator, (5) Condenser, (6) Back pressure regulator and (7) Wet gas meter.

1. One-dimensional plug flow fixed-bed reactor
2. The furnace temperature was assumed to be constant
3. Heat transfer by conduction was considered to be negligible compared to that of convection
5. Ideal gases
6. Steady-state conditions.

In the reactor model the mass and energy balances are derived for gas and solid phases separately. The mass balance for the gas phase species reads as follows:

Gas phase species balance

$$\text{Input - output} + \text{generation} - \text{consumption} = \text{accumulation} \Rightarrow 0 \tag{6}$$

$$f_t \cdot y_i|z - f_t \cdot y_i|z + \Delta z - a_v c_t k_{gi}(y_{is} - y_i) \cdot A_c \Delta z = 0 \tag{7}$$

$$\frac{f_t}{A_c}\left(\frac{y_i|z}{\Delta z} - \frac{y_i|z+\Delta z}{\Delta z}\right) - a_v c_t k_{gi}(y_{is} - y_i) = 0 \overset{\times -1}{\Rightarrow} \tag{8}$$

$$\lim_{\Delta z \to 0} \frac{y'_{(z+\Delta z)} - y_{(z)}}{\Delta z} = \frac{dy}{dz} \tag{9}$$

$$-\frac{f_t}{A_c}\frac{dy_i}{dz} + a_v c_t k_{gi}(y_{is} - y_i) = 0 \tag{10}$$

Gas phase energy balance

The energy balance of the gas phase is presented as follows:

$$f_t \cdot C_{pg} T|z - f_t \cdot C_{pg} T|z+\Delta z - a_v h_f (T_s - T) \cdot A_c \Delta z - \pi \cdot D_o \cdot \Delta z \cdot U(T_f - T) = 0 \tag{11}$$

$$\frac{f_t \cdot C_{pg}}{A_c}\left(\frac{T|z}{\Delta z} - \frac{T|z+\Delta z}{\Delta z}\right) - a_v h_f (T_s - T) - UA_t(T_f - T) = 0 \overset{\times -1}{\Rightarrow} \tag{12}$$

$$\lim_{\Delta z \to 0} \frac{T'_{(z+\Delta z)} - T_{(z)}}{\Delta z} = \frac{dT}{dz} \tag{13}$$

$$-\frac{f_t}{A_c} C_{pg} \frac{dT}{dz} + a_v h_f (T_s - T) + UA_t(T_f - T) = 0 \tag{14}$$

where y_i and T are the components mole fraction and temperature in the reactor, respectively, and y_{is} and Ts are the components mole fraction and temperature on catalyst surface.

Overall heat transfer coefficient, UA_t, can be estimated by Eq. (15).

$$UA_t = \left(\frac{\ln \frac{D_f}{D_o}}{2\pi K_w L} + \frac{1}{h_o \pi D_o L}\right)^{-1} \tag{15}$$

where D_f and D_o are furnace and reactor outside diameters, respectively. L is the reactor length, K_w is thermal conductivity and h_o is heat transfer coefficient of gas phase which is calculated according to Eq. (16) [47].

$$h_o = \frac{K_w}{D_p}\left(2.58\, Re^{1/3} Pr^{1/3} + 0.094\, Re^{0.8} Pr^{0.4}\right) \tag{16}$$

where Re and Pr are presented in Eqs. (17) and (18) as follows:

$$Re = \frac{\rho_g u_g D_p}{\mu_g} \tag{17}$$

$$Pr = \frac{C_{pg}\mu_g}{K_w} \tag{18}$$

The behavior of bulk gas is assumed to be ideal, thus the gas density can be calculated by Eq. (19).

$$\rho_g = \frac{Mw P}{RT} \tag{19}$$

where Mw is the average molecular weight of bulk gas. The molecular weight of each component is presented in Table A.2.1.

Gas velocity, u_g, which depends on space velocity at inlet condition, S_v in Eq. (20), is calculated by Eq. (21).

$$u_g = \frac{m_c S_v}{A_c \varepsilon_b} \tag{20}$$

$$S_v = S_{v0} \times \frac{T_0}{273.15} \times \frac{101325}{P_0} \tag{21}$$

where S_{v0} is the space velocity at standard temperature and pressure (STP).

The bed porosity can be calculated by Eq. (22) [48].

$$\varepsilon_b = 0.38 + 0.073\left(1 - \frac{\left(\frac{D_o}{D_p} - 2\right)^2}{\left(\frac{D_o}{D_p}\right)^2}\right) \tag{22}$$

Boundary conditions for the gas phase are expressed as:

$$z = 0 \quad y_i = y_{in} \quad T = T_{in} \tag{23}$$

Governing equations in catalyst pellets

Mass and energy balance equations for the solid phase (catalyst pellets) can be formulated as follows:

$$k_{gi} a_v c_t (y_i - y_{is}) + \rho_B \eta r_i = 0 \quad (\text{i} = \text{component number}) \tag{24}$$

$$a_v h_f (T - T_s) + \rho_B \eta \sum_{j=1}^{9} r_i \Delta H_{fj} = 0 \quad (\text{j} = \text{reaction number}) \tag{25}$$

where η is effectiveness factor, ΔH_{fj} is reaction enthalpy and ρ_B is the bulk density which can be calculated by Eq. (26).

$$\rho_B = (1 - \varepsilon_b)\rho_p \tag{26}$$

where ρ_p is the particle density. The important correlations for calculation of physical properties are presented in Appendix A.

Reaction rates/equilibrium

The kinetic rate equations for RWGS and FT reactions would be justified according to the mechanism reported in Table 4 [38]. Lack of kinetic parameters for all proposed FT reactions, persuade us to estimate them.

The LHHW mechanism is admitted to achieve kinetic rate equations. According to the elementary reactions and carbon chain distribution methods, the mechanisms for

Table 4 – Elementary steps of CO_2 hydrogenation presented to derive the kinetic model proposed by Saeidi et al. [38].

No	Elementary reactions
CO_2 shift	
1	$CO_2 + * \leftrightarrow CO_2*$
2	$CO_2* + H_2 \leftrightarrow CO* + H_2O$ (RDS)
3	$CO* \leftrightarrow CO + *$
	$CO_2 + H_2 \leftrightarrow CO + H_2O$
FT	
1	$CO + * \leftrightarrow CO*$
2	$H_2 + 2* \leftrightarrow 2H*$
3	$CO* + H_2 \rightarrow CHOH* + *$ (RDS)
4	$CHOH* + H* \leftrightarrow CH* + H_2O + *$
5	$CH* + H* \leftrightarrow CH_2* + *$
6	$CH_2* \leftrightarrow -CH_2- + *$
	$CO + 2H_2 \leftrightarrow -CH_2- + H_2O$

RWGS and FT were proposed and presented in Table 4. In order to determine each kinetic rate equation, the slowest step that controls total reaction rate should be considered as the rate determining step (RDS). For CO_2 shift reaction, the RDS is reaction between atomic adsorbed hydrogen and molecular CO_2, while for FT synthesis the RDS is the reaction between molecular hydrogen and adsorbed CO that results in the formation of hydroxyl methylene (CHOH*) as intermediate. Moreover, over catalyst surface the CO concentration is higher than that of hydrogen as a result of stronger CO adsorption over Fe.

Finally, fitting the experimental data and kinetic rate equations, the reaction and adsorption coefficients can be estimated via ABC and DE optimization algorithms.

The CO_2 hydrogenation components include H_2, CO_2, CO, H_2O, CH_4, C_2H_4, C_2H_6, C_3H_6, C_3H_8, C_4H_8 and C_4H_{10}. The following reactions (Table 5) are taken into consideration as the dominant reactions [27,49]. Accordingly, the employed rate equations which are the main engines of this mathematical model, are presented in Table 5.

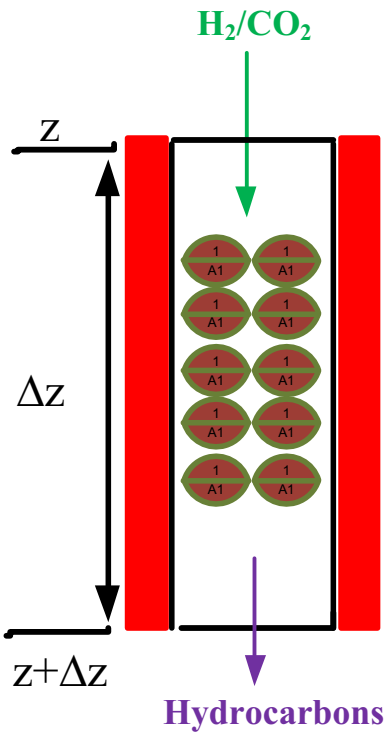

Fig. 2 – Schematic diagram of an elemental volume in the reactor.

Algorithms used to estimate kinetic parameters

Artificial Bee Colony (ABC) algorithm

In this section, an optimization method based on mimicking the chemical reactions in nature was introduced. The main features of this algorithm are the exploiting/exploring mechanisms combined with the elitist survival strategy, these features can reduce the chance that the algorithm stagnates in local optima. The performance of the chemical reaction

Table 5 – Proposed rate equations for each components in the current research.

Reaction types		Rate equations
CO_2 shift	$CO_2 + H_2 \leftrightarrow CO + H_2O$	$r_{sH} = k_{sH} \frac{P_{CO_2}P_{H_2} - P_{CO}P_{H_2O}/K_{eq}}{P_{CO} + a_{sH,H_2O}P_{H_2O} + b_{sH,CO_2}P_{CO_2}}$
FT (CH_4)	$CO + 3H_2 \rightarrow CH_4 + H_2O$	$r_{FT_{CH_4}} = k_{FT_{CH_4}} \frac{P_{CO}P_{H_2}}{P_{CO} + a_{FTCH_4,,H_2O}P_{H_2O} + b_{FT_{CH_4},CO_2}P_{CO_2}}$
FT (C_2H_4)	$2\,CO + 4\,H_2 \rightarrow C_2H_4 + 2\,H_2O$	$r_{FT_{C_2H_4}} = k_{FT_{C_2H_4}} \frac{P_{CO}P_{H_2}}{P_{CO} + a_{FT_{C_2H_4},H_2O}P_{H_2O} + b_{FT_{C_2H_4},CO_2}P_{CO_2}}$
FT (C_2H_6)	$2\,CO + 5\,H_2 \rightarrow C_2H_6 + 2\,H_2O$	$r_{FT_{C_2H_6}} = k_{FT_{C_2H_6}} \frac{P_{CO}P_{H_2}}{P_{CO} + a_{FT_{C_2H_6},H_2O}P_{H_2O} + b_{FT_{C_2H_6},CO_2}P_{CO_2}}$
FT (C_3H_6)	$3\,CO + 6\,H_2 \rightarrow C_3H_6 + 3\,H_2O$	$r_{FT_{C_3H_6}} = k_{FT_{C_3H_6}} \frac{P_{CO}P_{H_2}}{P_{CO} + a_{FT_{C_3H_6},H_2O}P_{H_2O} + b_{FT_{C_3H_6},CO_2}P_{CO_2}}$
FT (C_3H_8)	$3\,CO + 7\,H_2 \rightarrow C_3H_8 + 3\,H_2O$	$r_{FT_{C_3H_8}} = k_{FT_{C_3H_8}} \frac{P_{CO}P_{H_2}}{P_{CO} + a_{FT_{C_3H_8},H_2O}P_{H_2O} + b_{FT_{C_3H_8},CO_2}P_{CO_2}}$
FT (C_4H_8)	$4\,CO + 8\,H_2 \rightarrow C_4H_8 + 4\,H_2O$	$r_{FT_{C_4H_8}} = k_{FT_{C_4H_8}} \frac{P_{CO}P_{H_2}}{P_{CO} + a_{FT_{C_4H_8},H_2O}P_{H_2O} + b_{FT_{C_4H_8},CO_2}P_{CO_2}}$
FT (C_4H_{10})	$4\,CO + 9\,H_2 \rightarrow C_4H_{10} + 4\,H_2O$	$r_{FT_{C_4H_{10}}} = k_{FT_{C_4H_{10}}} \frac{P_{CO}P_{H_2}}{P_{CO} + a_{FT_{C_4H_{10}},H_2O}P_{H_2O} + b_{FT_{C_4H_{10}},CO_2}P_{CO_2}}$
DH	$nCO_2 + 3nH_2 - \rightarrow (CH_2)_n + 2nH_2O$	$r_{DH} = k_{DH} \frac{P_{CO_2}P_{H_2}}{P_{CO} + a_{DH,H_2O}P_{H_2O} + b_{DH,CO_2}P_{CO_2}}$

algorithm was evaluated on a set of complex benchmark functions and compared with other optimization algorithms. Simulation results displayed how the algorithm was able to reach near to the optimal values for some functions, performing better than the previously stated models, but more tests are needed to compare against some other algorithms that are proved to seek good solutions for larger dimensions [50].

Parameter identification is a crucial step in establishing kinetic models. Thus, it can be transformed into an optimization problem by constructing an objective function (O.F) that minimizes simulation errors. In the beginning, some traditional optimization techniques were employed to solve it such as the multivariable regression, the gradient-based optimization method, coordinate transformation, simplex and so on. Owing to the multi-dimensional characteristic and complex nonlinear relations, they were easy to trap into local optima.

Karaboga [51] proposed the ABC algorithm, for optimizing numerical problems, simulates the intelligent foraging behavior of honey bee swarms. As shown in Fig. 3 the flowchart of the ABC algorithm, the colony of artificial bees contains three groups of bees: employed bees; the honey bees which find food source, and unemployed bees: onlookers; the honey bees which wait in the dance area and make decision to choose food source and scouts; the honey bees which carry out stochastic search. In ABC, first half of the colony consists of employed artificial bees and the second half composes the artificial onlookers. The employed bee whose food source has been exhausted becomes a scout bee. The position of a food source demonstrates a feasible solution to the optimization problem and the nectar amount of a food source corresponds to the quality (fitness) of the associated solution. The number of the employed bees is equal to the number of food sources, each of which also represents a site, which is exploited at the moment. More detailed explanation about ABC algorithm can be found in Appendix B, B.1.

Differential Evolution (DE) algorithm

The DE algorithm is a population based algorithm similar to GA employing the same operators: mutation, crossover, and selection. The principal discrepancy in constructing better

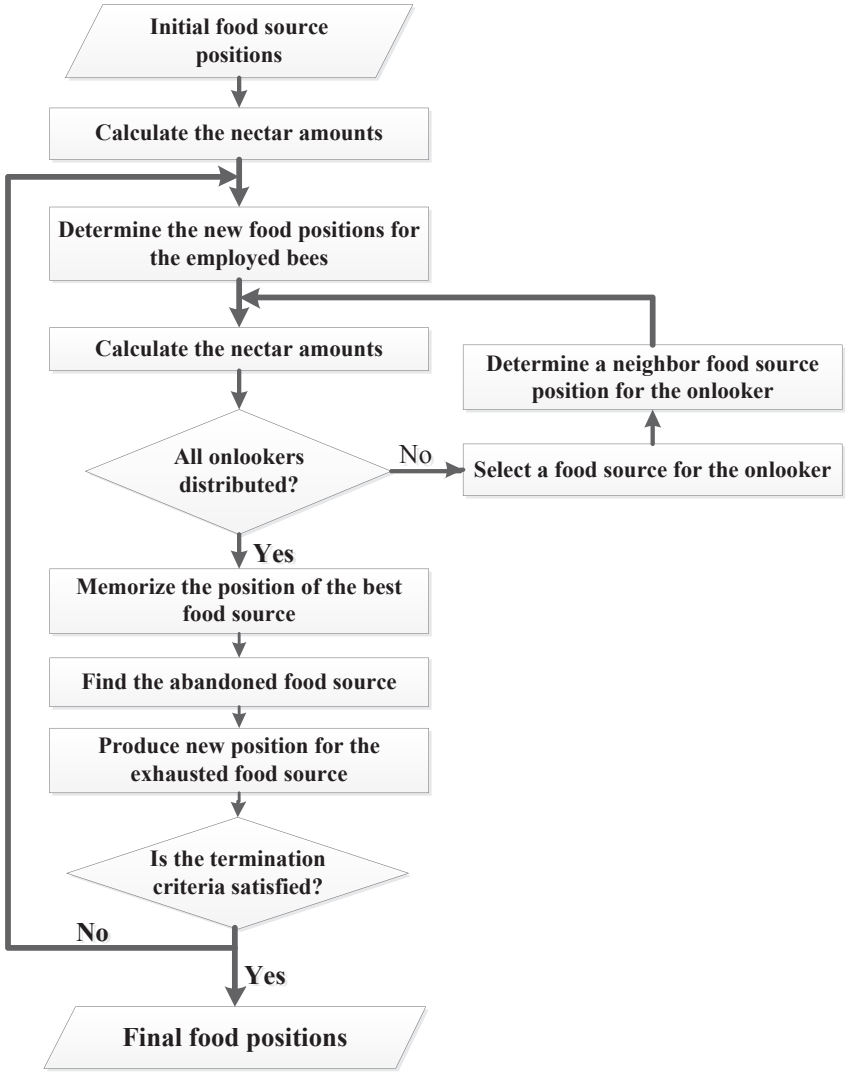

Fig. 3 – The ABC algorithm flowchart [51].

solutions is that GA depends on crossover while DE relies on mutation operation. This main operation is founded on the differences of randomly sampled pairs of solutions in the population.

As illustrated in Fig. 4, DE algorithm uses mutation operation as a seeking mechanism and selection operator to direct the search toward the probable regions in the search space. A non-uniform crossover is exploited by DE algorithm for obtaining child vector parameters, where among all parents one is usually being employed more. Employing the components of the existing population members to create trial vectors, the recombination (crossover) operator efficiently shuffles data about appropriate combinations, enabling the search for a better solution space [52].

An optimization task consisting of D parameters can be represented by a D-dimensional vector. In DE, initially a population of near optimal solution vectors is randomly created. This population is proficiently enhanced via applying mutation, crossover, and selection operators. The main steps of the DE algorithm are illustrated in Fig. 4 [53,54]. More detailed explanation about DE algorithm can be found step by step in Appendix B, B.2.

Results and discussion

Comparison between the two algorithms

In order to evaluate the accuracy of the two proposed algorithms, the results of predictions were compared to those obtained via experimental tests for the conversion of H_2 and CO_2 along with products distribution. As shown in Table 6, the low conversion of CO_2 (X_{CO2}) refers to the nature of CO_2 indeed, due to, chemical and thermodynamic stability of CO_2 molecule. It is a multi-reaction system, CO_2 as feed must be converted to CO based on RWGS reaction; and then CO would be proceeded to hydrocarbons according to FT reactions. Meanwhile, hydrogen is fed for both of the reactions (RWGS & FT).

Moreover, it should be noted that these results are based on the proposed model in which the estimated kinetic parameters are obtained with the goal of minimization of errors between experimental and predicted hydrocarbons yield. On the other hand, some non-idealities regarding catalyst deactivation or/and the effect of other parameters in the reduction of CO_2 conversion as the main carbon source are not included in the model to avoid further complexity. For instance, the coke formation according to the Boudouard reaction (Eq. (27)) hampers the catalytic formation of hydrocarbons has not been considered since the temperature is below 633 K. In addition, ABC algorithm is highly dependent on the initial guess as well as the defined upper and lower bounds of the variables which are set according to the data reported by Riedel et al. [27]. It is noteworthy, the kinetic parameters of the FT reactions were estimated for C_3H_6 as the sole hydrocarbon product of this process by Riedel et al. [27]. However, seven components consisting CH_4, C_2H_4, C_2H_6, C_3H_6, C_3H_8, C_4H_8 and C_4H_{10} are considered as the products of FT reactions in the present study. Therefore, it is expected to observe such deviation in the conversion of CO_2 in experiments compared to the

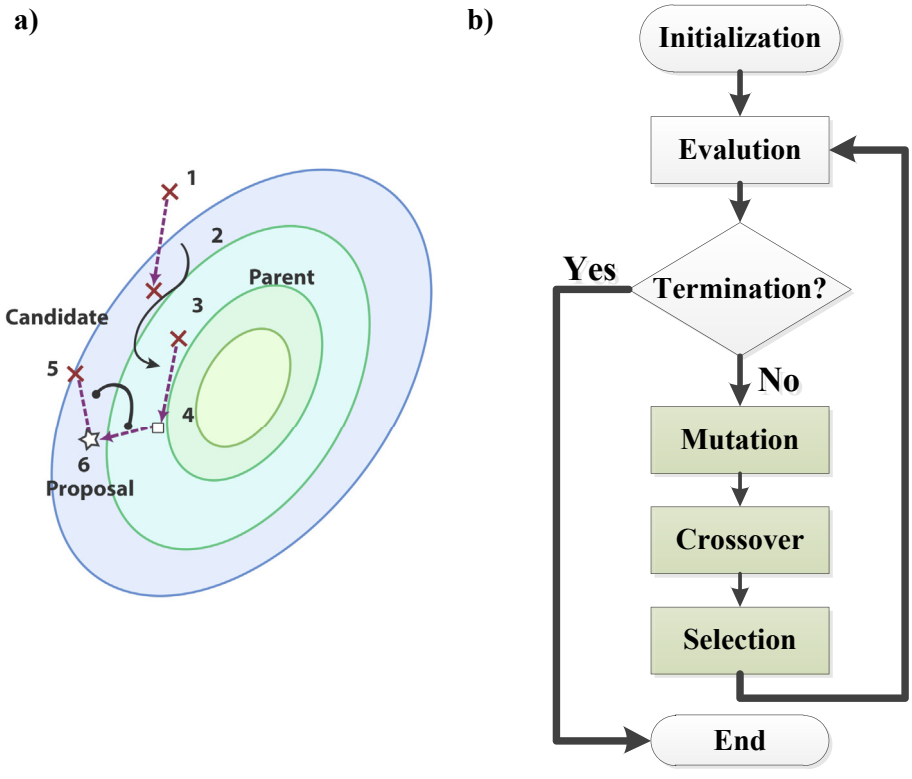

Fig. 4 – Differential evolution algorithm a) pattern of finding a new proposal b) flowchart [53,54].

Table 6 – Comparison between experimental and predicted results of ABC and DE algorithms for fresh Fe–K/γ-Al_2O_3 catalyst.

Parameters	Experimental results	ABC prediction results	ABC Relative error (%)	DE prediction results	DE Relative error (%)
X_{CO_2}	52.17	87.1	66.95	87.52	67.76
X_{H_2}	89.20	90.82	1.82	90.99	2.00
S_{CO}	14.45	15.57	7.75	19.12	32.31
SCH_4	16.30	16.18	0.74	18.90	15.95
SC_2H_4	17.90	18.1	1.12	15.19	15.15
SC_2H_6	3.28	3.18	3.05	4.38	33.54
SC_3H_6	20.64	19.87	3.73	22.14	7.27
SC_3H_8	2.34	2.57	9.83	3.88	65.60
SC_4H_8	10.82	11.78	8.87	7.80	27.94
SC_4H_{10}	1.31	1.53	16.79	2.16	64.89
S_{HC}	72.59	73.21	6.3	74.45	32.9

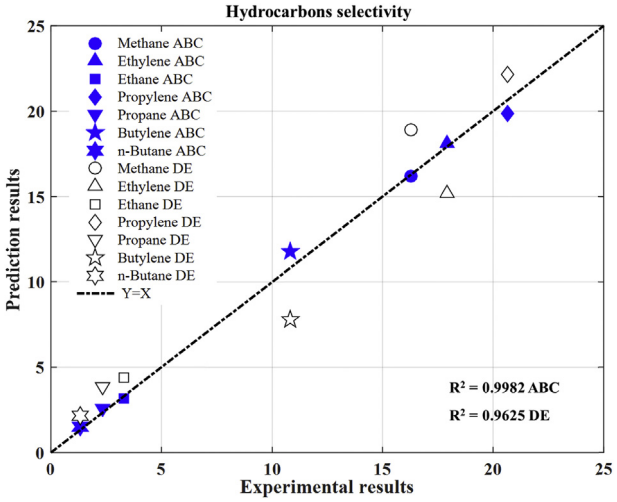

Fig. 5 – Prediction versus experimental results for hydrocarbons selectivity.

ideal model. However, errors in the calculation of products selectivity exploiting ABC algorithm are within an acceptable range, and the products distribution are in accordance with the previously reported trends in literature [39,55–58] for Fe–K/γ-Al_2O_3 catalysts. It is worth mentioning that the high errors corresponding to DE algorithm are due to its inefficiency compared to ABC algorithm. According to the results presented in Table 6 relative errors of ABC algorithm are generally lower compared to those of DE algorithm.

$$CO + CO \leftrightarrow C_{(s)\downarrow} + CO_2 \quad \Delta H_{573\ K} = 173.5\ kJ/mol \tag{27}$$

The superiority of the ABC algorithm can be inferred from Fig. 5 as well which, illustrates the appropriate regression coefficient of ABC algorithm in estimating the hydrocarbons selectivity.

Calculation of kinetic parameters

Reaction constants described in terms of pre-exponential factors, k_i, activation energies, E_i, and equilibrium constant of CO_2 shift reaction, K_{eq}, are indicated in Table 7.

Utilizing the ABC algorithm and experimental data of the present study, the kinetic parameters can be estimated via minimization of the O.F as described in Eq. (28). Accordingly, unknown parameters in the rate equations are estimated and presented in Table 8. The flowchart for calculation of kinetic parameters is demonstrated in Fig. 6.

Table 7 – Reaction constants and the corresponding parameters.

Rate number	Reactions	Reaction constants	Unknown parameters
r_1	CO_2 Shift	$k_{sH} = k_1\ exp\left(-\frac{E_1}{RT}\right), \log(K_{eq}) = \left(\frac{B_1}{T} - B_2\right)$	$\{k_1, E_1, B_1, B_2, a_{sH,H_2O}, b_{sH,CO_2}\}$
r_2	FT (CH_4)	$k_{FT_{CH_4}} = k_2\ exp\left(-\frac{E_2}{RT}\right)$	$\left\{k_2, E_2, a_{FT_{CH_4}.H_2O}, b_{FT_{CH_4}.CO_2}\right\}$
r_3	FT (C_2H_4)	$k_{FT_{C_2H_4}} = k_3\ exp\left(-\frac{E_3}{RT}\right)$	$\left\{k_3, E_3, a_{FT_{C_2H_4}.H_2O}, b_{FT_{C_2H_4}.CO_2}\right\}$
r_4	FT (C_2H_6)	$k_{FT_{C_2H_6}} = k_4\ exp\left(-\frac{E_4}{RT}\right)$	$\left\{k_4, E_4, a_{FT_{C_2H_6}.H_2O}, b_{FT_{C_2H_6}.CO_2}\right\}$
r_5	FT (C_3H_6)	$k_{FT_{C_3H_6}} = k_5\ exp\left(-\frac{E_5}{RT}\right)$	$\left\{k_5, E_5, a_{FT_{C_3H_6}.H_2O}, b_{FT_{C_3H_6}.CO_2}\right\}$
r_6	FT (C_3H_8)	$k_{FT_{C_3H_8}} = k_6\ exp\left(-\frac{E_6}{RT}\right)$	$\left\{k_6, E_6, a_{FT_{C_3H_8}.H_2O}, b_{FT_{C_3H_8}.CO_2}\right\}$
r_7	FT (C_4H_8)	$k_{FT_{C_4H_8}} = k_7\ exp\left(-\frac{E_7}{RT}\right)$	$\left\{k_7, E_7, a_{FT_{C_4H_8}.H_2O}, b_{FT_{C_4H_8}.CO_2}\right\}$
r_8	FT (C_4H_{10})	$k_{FT_{C_4H_{10}}} = k_8\ exp\left(-\frac{E_8}{RT}\right)$	$\left\{k_8, E_8, a_{FT_{C_4H_{10}}.H_2O}, b_{FT_{C_4H_{10}}.CO_2}\right\}$
r_9	DH	$k_{DH} = k_9\ exp\left(-\frac{E_9}{RT}\right)$	$\{k_9, E_9, a_{DH,H_2O}, b_{DH,CO_2}\}$

Table 8 – Kinetic parameter values as determined through ABC algorithm for Fe–K/γ-Al_2O_3 at 1 MPa, T = 573 K.

Reaction	a_{H_2O}	b_{CO_2}	k (mol/(s.g.MPa))	E(kJ/mol)
CO_2 Shift	53.4768	4.5697	0.6196 E8	136
FT (CH_4)	43.0480	3.4174	0.3817 E8	135
FT (C_2H_4)	41.1777	3.1104	4.0918 E8	146
FT (C_2H_6)	85.9319	2.3182	0.4931 E8	141
FT (C_3H_6)	15.9468	4.0486	2.5451 E8	147.1
FT (C_3H_8)	55.5611	3.1525	0.0142 E8	127
FT (C_4H_8)	30.9173	4.9477	0.0014 E8	111
FT (C_4H_{10})	87.9118	3.7471	84.4447	81
DH	74.3470	62.0165	36.5745	150

$$O.F = Min\frac{1}{N}\sum_{i=1}^{N}\left(y_{exp,i} - y_{model,i}\right)^2 \quad (28)$$

The values determined for kinetic parameters reported by Riedel et al. [27] are presented in Table 9. The differences in our estimated values with those of the available report can be attributed to various factors such as reactor volume and catalyst properties.

Comparison of modeling results with various literature data

The results of the modeling exploiting the kinetic parameters calculated via both ABC and DE algorithms are compared with experimental data of literature and illustrated in Fig. 7a–g. To this aim, seven sets of experimental data from previous studies are used. Each set of data is nominated by a code (A to H) which includes the reaction conditions and catalyst as presented in Table 10.

Fig. 7a–g illustrate seven different hydrocarbon products (i.e. methane, ethylene, ethane, propylene, propane, butylene and butane) in terms of selectivity via model prediction and literature data (colored bars) over various catalysts containing Fe and K supported on γ-Al_2O_3. Calculation of relative errors shows that the predicted results of ABC algorithm exhibiting 6.3% error are in good accordance with the experimental data compared to those of DE. The difference of predictions with available experimental data presented as error refers to different catalysts with various BET surface areas as a result of diversities in catalyst synthesis methods along with differences in reactor dimensions. Comparison of the products distribution with recently reported catalysts can be observed in Table 11. It is obvious that catalyst characteristics and reaction conditions have crucial roles in products distribution.

Model analysis

The proposed model is solved using MATLAB codes according to the algorithm which is presented in Fig. 8. Yields of CO and

Table 9 – Parameter values determined by Riedel et al. [27] for Fe–K–Cu/Al_2O_3 at 1 MPa, T = 573–633 K.

Reaction	a_{H_2O}	b_{CO_2}	k (mol/(s.g.MPa))	E(kJ/mol)
CO_2 Shift	65	7.4	0.151 E8	55
FT	33	2.7	2.58 E8	72
DH	90	66	39.6	20

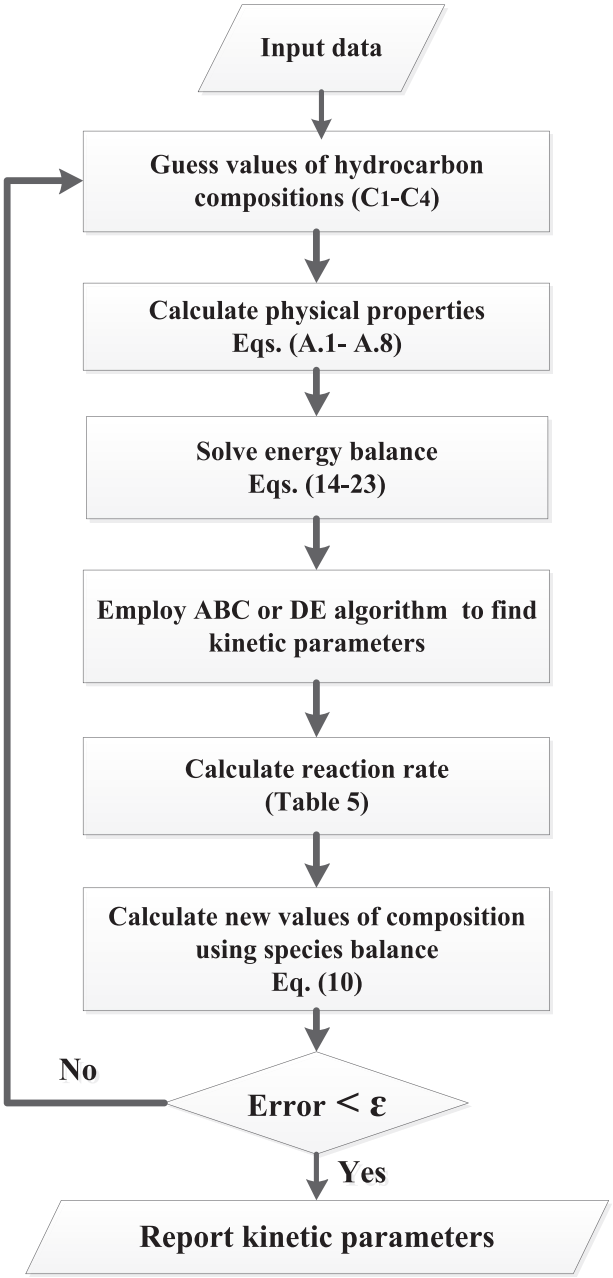

Fig. 6 – Algorithm for the estimation of kinetic parameters.

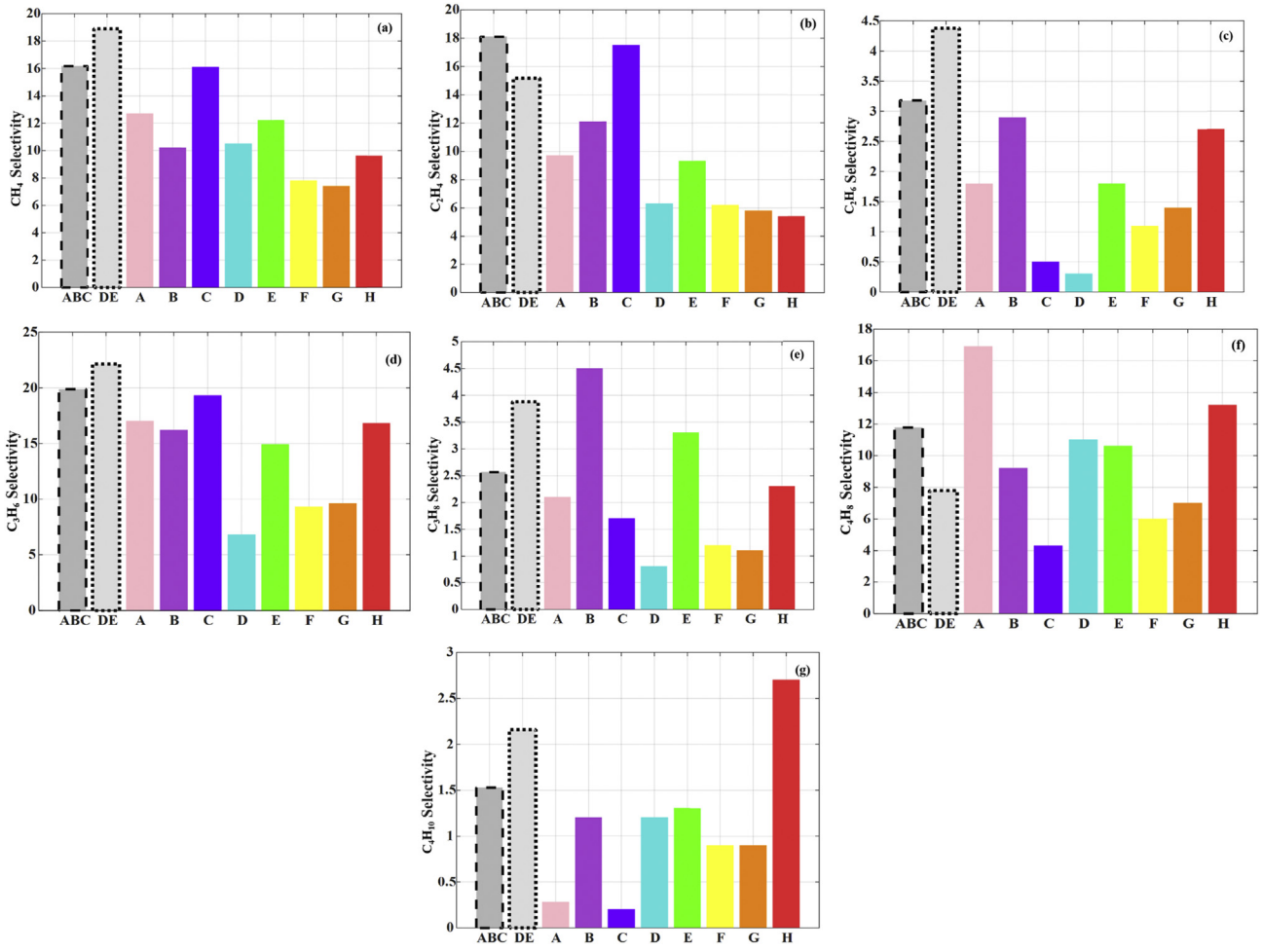

Fig. 7 – Comparison of modeling and literature data for selectivity of a) Methane, b) Ethylene, c) Ethane, d) Propylene, e) Propane, f) Butylene and g) Butane.

Table 10 – Conditions corresponding to each code.

Code	Catalyst	BET (m^2/g)	T (K)	P (MPa)	SV ($ml/g_{cat}.h$)	Ref.
ABC	Fe–K/γ-Al_2O_3	136	573	1	2000	Present study
DE	Fe–K/γ-Al_2O_3	136	573	1	2000	Present study
A	Fe–K/γ-Al_2O_3	NA	573	1	1896	[58]
B	Fe–K/γ-Al_2O_3	133	573	1	2000	[39]
C	Fe–K/γ-Al_2O_3 (Al binder)	132	573	1	2000	[39]
D	Fe–K/γ-Al_2O_3 (PVA binder)	146	573	1	2000	[39]
E	Fe–K/γ-Al_2O_3 (Silica binder)	110	573	1	2000	[39]
F	Fe–K/γ-Al_2O_3	92	588	1.5	2000	[55]
G	Fe–K/γ-Al_2O_3 (PVA binder)	92	573	1	1000	[57]
H	Fe–K/γ-Al_2O_3 (PVA binder)	124.5	573	1	500	[56]

produced hydrocarbons at different times are depicted along the reactor length (Fig. 9).

Fig. 9 illustrates the trend of CO and hydrocarbon yields along the reactor. Accordingly, after 24 h the order of produced hydrocarbons are propylene, ethylene, methane, butylene, ethane, propane and butane, respectively. It can be seen that at short reaction times propylene and ethylene compete for being the main product while at longer times propylene exceeds which is illustrated in Fig. 10. Besides it can be observed that the olefin production prevails those of paraffins as can be seen in Fig. 11.

The trend of olefin and paraffin distribution

The trend of olefin/paraffin ratio considerably varies during lower reaction times whereas it changes slightly during last 10 h (Fig. 8).

Table 11 – Comparing products distribution with available experimental results at $H_2/CO_2 = 3$.

Catalyst	CH_4	CO	Total olefins ($C_2H_4+C_3H_6+C_4H_8$)	Total paraffins ($C_2H_6+C_3H_8+C_4H_{10}$)	Ref.
Fe–K/γ-Al_2O_3	16.18	19.7	49.82	7.24	Present study
Fe/SiO_2	44.1	6.5	1.5	47.9	[59]
α-Fe_2O_3	27.5	17	30	18	[60]
γ-Fe_2O_3/Fe_3O_4					
Fe–K/γ-Al_2O_3	18	22	25	11	[61]
Fe-(Mn, K)/γ-Al_2O_3	16.1	28	56		[20]
Fe-M/Al_2O_3	29	–	71		[62]
M = Co, Ni, Cu, Pd					
Fe–Cu–K/γ-Al_2O_3	7	17	76		[63]

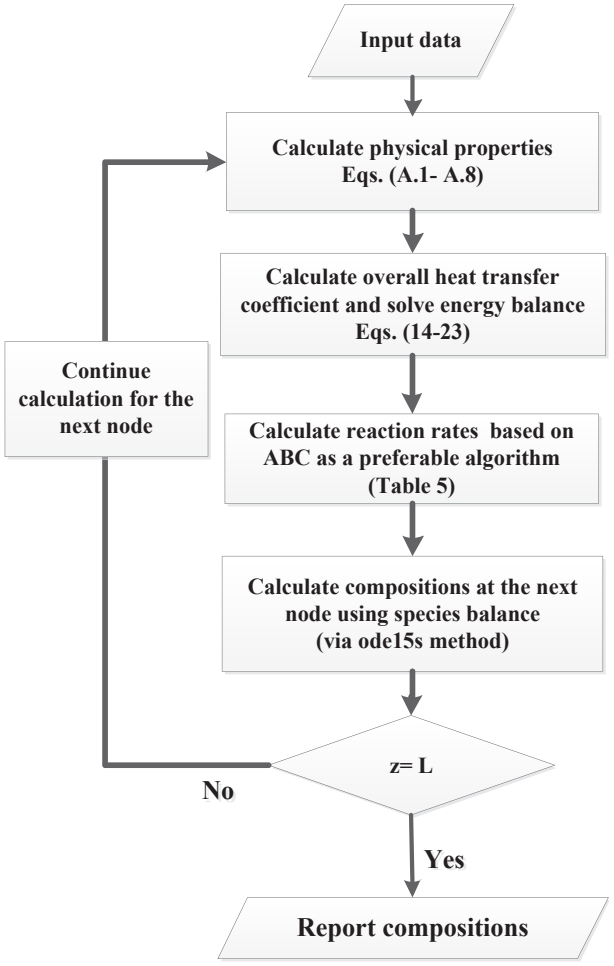

Fig. 8 – Algorithm for solving governing equations.

Fig. 11 depicts that olefin/paraffin ratio increases gradually with time and this ratio is evidently higher when carbon number is grater than three.

Formation and consumption of CO along the reactor

Moreover, as can be seen in Fig. 9, CO is formed rapidly and then consumes gradually. Evidently, a definite CO concentration in the reactor is required for hydrocarbon production, and the peak in CO yield indicates the point that enough CO is produced for the beginning of FT reactions. Accordingly, hydrocarbon yields increase dramatically for all components at the reactor entrance which are attributed to the CO formation and then slightly increase in the rest of the reactor length due to CO consumption and finally remain constant due to gradual deterioration of the reactants and RWGS equilibrium. This can be seen also in Fig. 12 which depicts the sharp increase in H_2 and CO_2 conversions and total hydrocarbon yield at reactor entrance at two different times. Besides, it is shown that the peak of CO yield becomes sharper and the final yield approaches to less values at longer times. This phenomenon is illustrated in Fig. 13 with more details.

As can be observed in Fig. 12, H_2 and CO_2 conversions dramatically increase at the reactor entrance (about 0.1 m) owing to RWGS reaction then slightly increase which refer to FT reaction occurrence and afterwards approach to approximately 90.8% and 87.1% in 24 h, respectively. However, CO_2 conversion slightly increases along the reactor, especially at short times which refers to chemical and thermodynamic stability of CO_2 molecule.

According to Fig. 13, the CO consumption rate becomes faster as time passes which can be attributed to the completion of FT reaction at longer times. At initial time steps, the RWGS reaction occurs and equilibrium reaches while the FT reaction cannot proceed due to the shortage of time and CO concentration. Therefore, at longer times, more hydrocarbons can be produced as a result of FT reaction which is obviously demonstrated in Fig. 12. It can be observed that the peak of CO yield decreases slightly at longer times, which may be an indication of reaching the reaction extent. In this situation, approximately all of CO component is consumed and reaction will not proceed more. The ratio of CO to CO_2 consumption (CO selectivity) along with CO_2 conversion versus time are shown in Fig. 14.

It can be realized that the rate of CO production dramatically reduces at lower times (before 1 h) while a slight decrease is occurred as time passes which is attributed to the slow consumption rate of CO_2 as a result of reaching equilibrium as can be detected in Fig. 14.

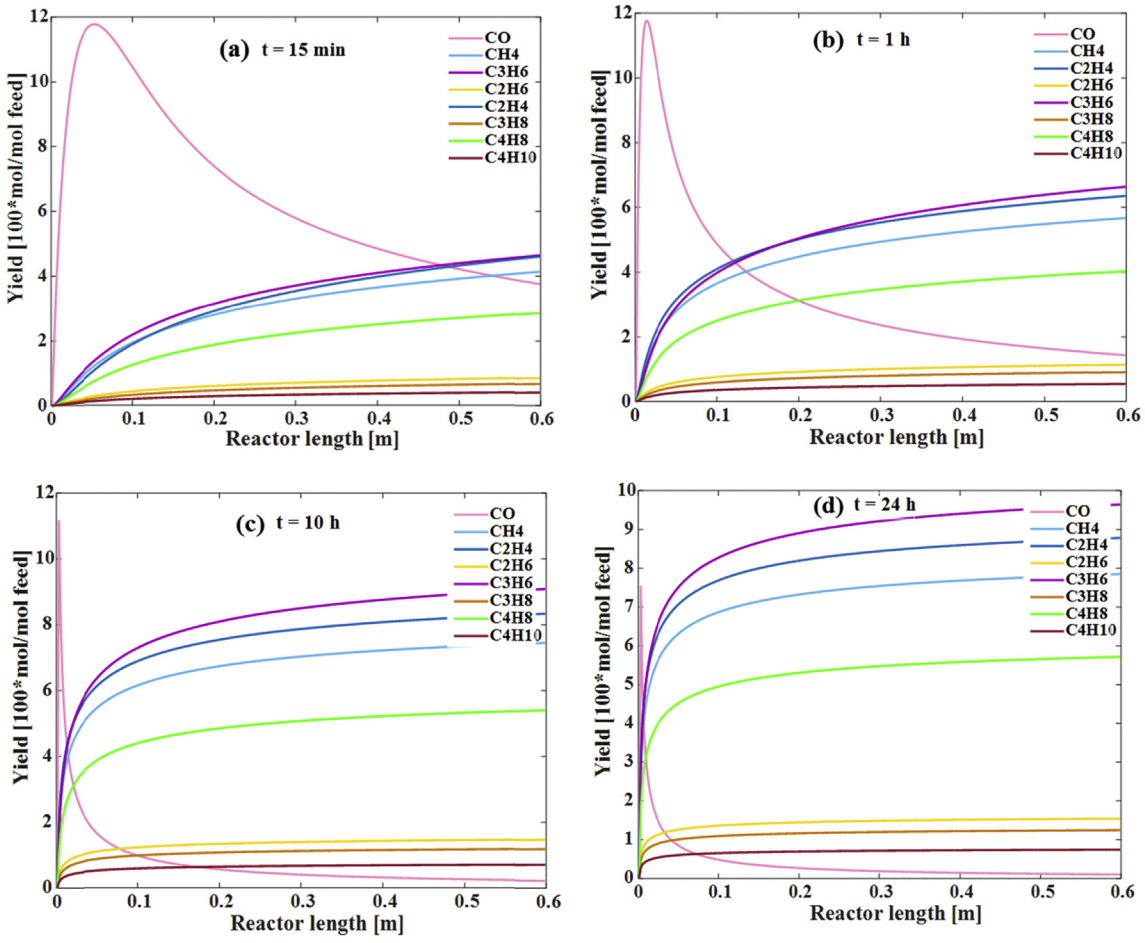

Fig. 9 – Yields of CO and produced hydrocarbons along the reactor length at 573 K a) 15 min, b) 1 h, c) 10 h and d) 24 h.

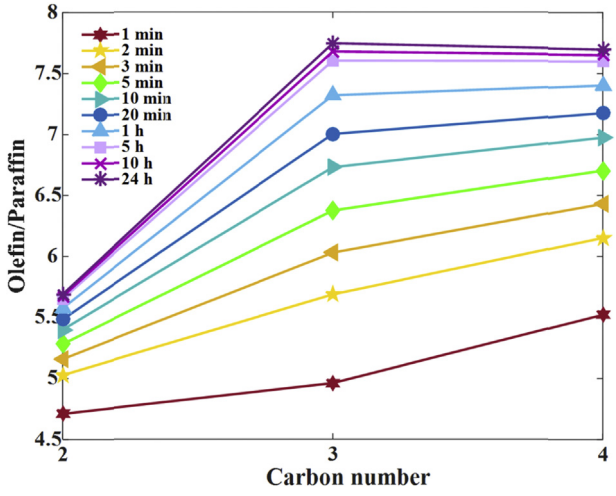

Fig. 10 – The trend of olefin/paraffin ratio for different carbon numbers at 573 K.

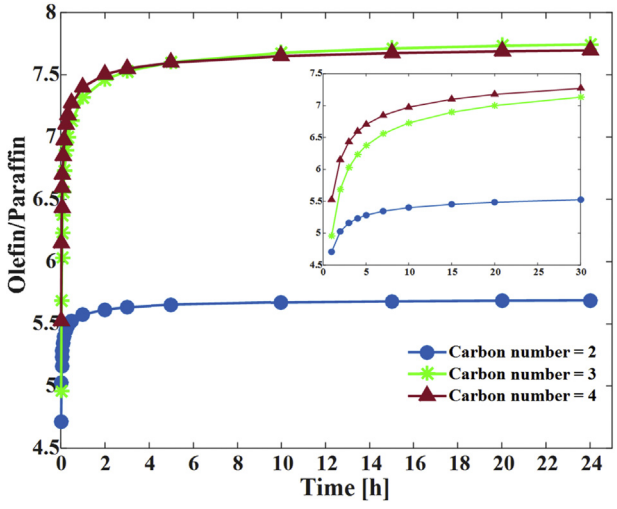

Fig. 11 – Evolution of olefin/paraffin ratio versus reaction time at 573 K.

Time dependency of reactor temperature

The temperature of the reactor changes suddenly at the reactor entrance. As depicted in Fig. 15, temperature of bulk gas decreases first as a result of endothermic RWGS and then a remarkable increase occurs due to exothermic FT reactions. In other words, since the reactor temperature is kept constant via utilization of a furnace, no heat source is available to start the endothermic RWGS reaction. Therefore, the reaction has

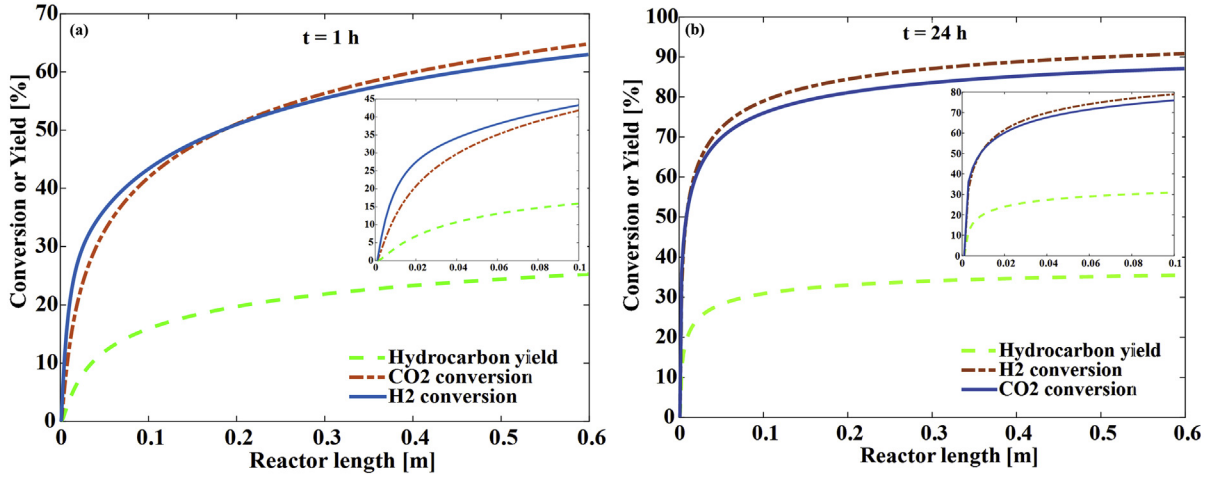

Fig. 12 – Feed conversion and hydrocarbons yield along the reactor length at 573 K a) 1 h, b) 24 h.

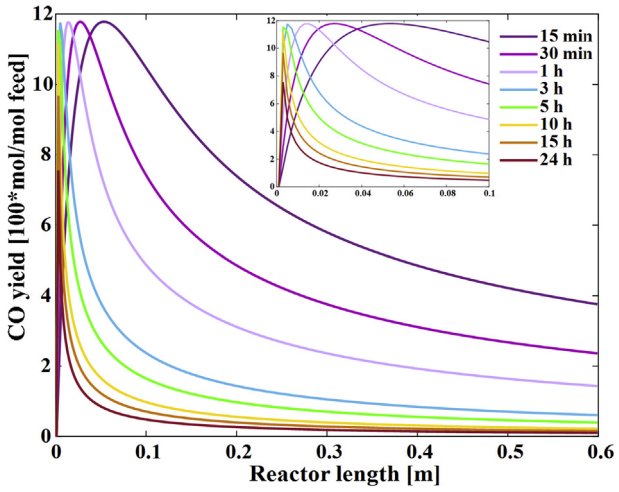

Fig. 13 – CO yield along reactor length at different times at 573 K.

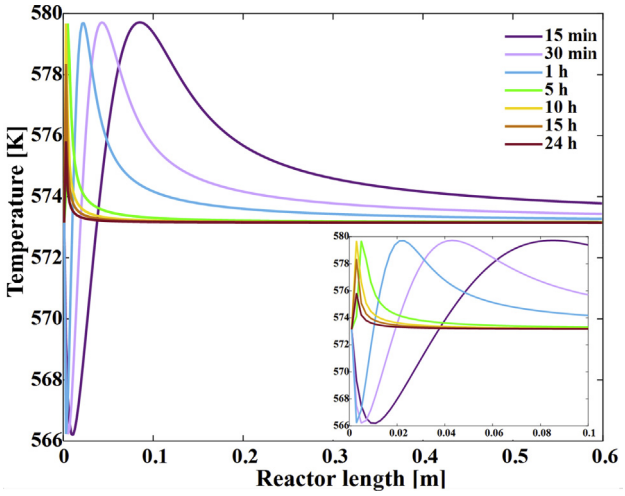

Fig. 15 – Temperature of bulk gas along the reactor length at 573 K.

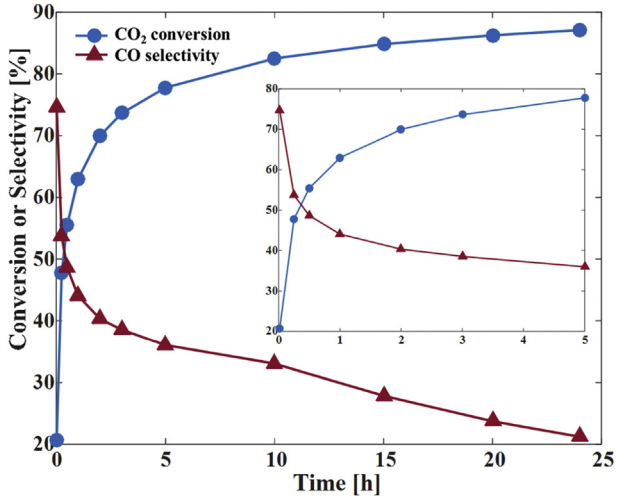

Fig. 14 – CO_2 conversion and CO selectivity versus time at 573 K.

to proceed utilizing the temperature of the bulk gas which leads to a sudden decrease in reactor temperature (hot spot). However, after a while CO is produced and FT reactions which are exothermic can proceed simultaneously while releasing the heat required for maintaining the reactor temperature as well as heat of endothermic RWGS.

It can be observed that as time passes the first peak vanishes while the second peak becomes sharper. This can be ascribed to the nature of RWGS reaction which occurs rapidly at initial seconds with respect to FT reactions. Indeed (as illustrated in Fig. 16), CO is required to be produced to some extent to act as the main feed of FT reactions. In other words at longer times (about 10 h) peak of CO yield occurs closer to the reactor entrance as a result of reached equilibrium while at initial times of reaction RWGS is the main reaction (since CO_2 and H_2 are more available than CO). Therefore, longer reactor length is required for the consumption and production of CO as an intermediate component which is required for the proceeding of FT reactions.

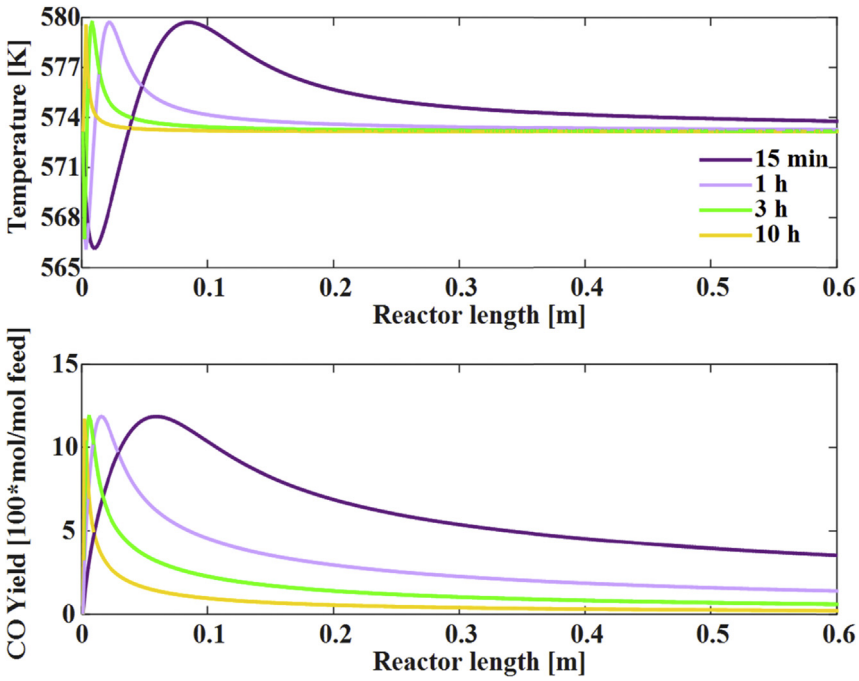

Fig. 16 – Temperature and CO yield along the reactor lenght at 573 K.

Conclusions

Results of one dimensional heterogeneous model for CO_2 hydrogenation fixed-bed reactor were compared with experimental results to estimate kinetic parameters via optimization. The results showed that ABC with average error of 6.3% was more reliable and accurate than DE algorithm with 32.9% error to predict hydrocarbons distibution. The kinetic parameters determined via applying ABC algorithm were approximately in accordance with those of reported in previous studies considering the varieties in catalyst properties and reaction conditions.

Exploiting the determined kinetic parameters, reactor performance for RWGS, FT and DH reactions was studied in the presence of Fe–K/γ-Al_2O_3. Experimental results could be well predicted via the provided model. Besides, reported results by various researchers were in good agreement with model predictions in terms of hydrocarbons selectivity. It was revealed that total hydrocarbons selectivity predicted by the proposed model (73.21%) was comparable to that of experimental results (72.56%) with an error of 0.85%. Results of model analysis revealed that propylene was the most efficient product and as a whole, catalyst acted more selective towards olefins compared to paraffins. Moreover, the olefin/paraffin ratio was higher in high carbon number hydrocarbons. It was found out that the CO production and consumption were dependent to the rates of RWGS and FT reactions, respectively which were affected by the equilibrium limitations at various temperatures. Moreover, illustration of reactor temperature at various time steps proved the occurrence of both endothermic RWGS and exothermic FT reactions in the reactor while giving a comprehensive insight about the temperature and time dependencies of CO yield.

Thus, the rigorous mathematical modeling is a fast, robust tool to investigate and predict the reactor performance while providing an extensive insight about influential parameters for designing advanced reactor configurations in CO_2 hydrogenation process. However, additional studies are ongoing to further investigate the contribution of significant factors on the reaction rates and products distribution.

Acknowledgements

This research was performed in the frame of FIEK_16-1-2016-0007 project, implemented with the support provided from the National Research, Development and Innovation Fund of Hungary, financed under the FIEK_16 funding scheme.

Nomenclatures

A_c	cross sectional area of reactor [m^2]
a_v	specific surface area of catalyst pellet [$m^2\ m^{-3}$]
a_{sH,H_2O}	inhibition coefficient for H_2O in shift reaction [-]
a_{FT_i,H_2O}	inhibition coefficient for H_2O in Fisher-Tropsch reaction [-]
a_{DH,H_2O}	inhibition coefficient for H_2O in direct hydrogenation reaction [-]
b_{sH,CO_2}	inhibition coefficient for CO_2 in shift reaction [-]
b_{FT_i,CO_2}	inhibition coefficient for CO_2 in Fisher-Tropsch reaction [-]
b_{DH,CO_2}	inhibition coefficient for CO_2 in direct hydrogenation reaction [-]
B_1	constant in K_{eq} equation [K]
B_2	constant in K_{eq} equation [-]

C_{pg} specific heat of the gas at constant pressure [J mol^{-1} K^{-1}]
c_t total concentration [mol m^{-3}]
D_0 reactor outside diameter [m]
D_f furnace diameter [m]
D_p particle diameter [m]
E_i apparent activation energy [kJ mol^{-1}]
f_s correction factor in Eq. (A.6) [-]
f_t total gas molar flow rate in reactor [mol s^{-1}]
h_0 gas-catalyst heat transfer coefficient [Wm^{-2} K^{-1}]
K_{eq} equilibrium constant of CO_2 shift reaction [-]
K_w thermal conductivity of reactor wall [Wm^{-1} K^{-1}]
k_i pre-exponential factor in Arrhenius law [mol s^{-1}g^{-1}MPa^{-1}]
k_{sH} reaction rate constant for shift reaction [mol s^{-1}g^{-1}MPa^{-1}]
k_{FT_i} reaction rate constant for Fisher-Tropsch reaction [mol s^{-1}g^{-1}MPa^{-1}]
k_{DH} reaction rate constant for direct hydrogenation reaction [mol s^{-1}g^{-1}MPa^{-1}]
k_{gi} mass transfer coefficient between gas and solid phase for component "i" [m s^{-1}]
L reactor length [m]
Mw molecular weight [mol/kg]
m_c catalyst weight [kg]
P_0 initial pressure [Pa]
P reactor pressure [Pa]
P_i pressure of component "i" [Pa]
R universal gas constant [J mol^{-1}K^{-1}]
Re Reynolds number [-]
r_i reaction rate of component "i" [mol mol^{-1} s^{-1}]
S_{v0} space velocity at standard temperature and pressure (STP) [m s^{-1}]
S_v space velocity at inlet condition [m s^{-1}]
T_0 initial gas temperature [K]
T bulk gas phase temperature [K]
$T_{B,i}$ boiling point of component "i" [K]
T_f temperature of furnace [K]
T_s temperature of solid phase [K]
UA_t overall heat transfer coefficient between jacket and gas phase [Wm^{-2} K^{-1}]
u_g linear velocity of gas phase [m s^{-1}]
v_r reactor volume [m^3]
y_i mole fraction of component "i" in the gas phase [mol mol^{-1}]
y_{is} mole fraction of component "i" in the solid phase [mol mol^{-1}]
S_i Sutherland constant of pure component "i" [K]
S_{ij} geometric mean of S_i and S_j [K]
z axial dimension [m]

Greek letters

η catalyst effectiveness factor [–]
μ_g viscosity of gas phase [kg m^{-1} s^{-1}]
ΔH_{fj} enthalpy of reaction j [J mol^{-1}]
ΔH_{298} enthalpy of reaction at 298 K [J mol^{-1}]
ρ_p density of catalyst [kg m^{-3}]
ρ_B density of catalytic bed [kg m^{-3}]
ε_b bed porosity [–]
θ_{ij} constant parameter in Eq. (A.5) [–]

Abbreviations

ABC Artificial Bee Colony
AC Ant Colony
AFS Artificial Fish Swarm
BET Brunauer–Emmett–Teller
DE Differential Evolution
DH Direct hydrogenation
ER Experimental Reactor
FT Fischer-Tropsch
GA Genetic Algorithm
GHSV Gas Hourly Space Velocity
GTL Gas to Liquid
HC Hydrocarbons
LHHW Langmuir-Hinshelwood-Hougen-Watson
O.F Objective Function
PSO Particle Swarm Optimization
PVA Poly Vinyl Alcohol
RWGS Reverse Water Gas Shift
RDS Rate Determining Step
SI Swarm intelligent
WGS Water Gas Shift

Appendix A

A.1 Important correlations for calculation of physical properties

According to pressure and temperature changes during reaction, physical properties are estimated via proper correlations.

Heat capacity

The heat capacity of mixture, C_{pg}, is calculated as the molar average heat capacity of each species, $C_{p,i}$, according to Eq. (A.1).

$$C_{pg} = \sum_{i=1}^{N} y_i C_{pg,i} \quad \text{(A.1)}$$

where $C_{pg,i}$ is the heat capacity of component "i" which can be estimated via the proposed correlation in Eq. (A.2).

$$C_{pg,i} = \left(A1_i + A2_i \times T + A3_i \times T^2 + A4_i \times T^{-2}\right) \times R \quad \text{(A.2)}$$

where A1, A2, A3 and A4 are constants which were provided in Perry and Green [64] and are presented in Table A.1.1.

Table A.1.1 – Constants for gas species corresponding to Eq. (A.2).

Component	A1	A2 × 10^{-3}	A3	A4 × 10^{-5}
H_2	3.249	0.422	0	0.083
CO_2	5.457	1.045	0	−1.157
CO	3.376	0.557	0	−0.031
CH_4	1.702	9.081	−2.164	0
C_2H_4	1.424	14.394	−4.392	0
C_2H_6	1.131	19.225	−5.561	0
C_3H_6	1.637	22.706	−6.915	0
C_3H_8	1.213	28.875	−8.824	0
C_4H_8	1.967	31.630	−9.873	0
C_4H_{10}	1.935	36.915	−11.402	0
H_2O	3.470	1.450	0	0.21

Thermal conductivity

Thermal conductivity of the bulk mixture can be calculated according to Eq. (A.3).

$$K_w = \sum_{i=1}^{N} \frac{y_i K_{w_i}}{\sum_{j=1}^{N} y_j \theta_{ij}} \tag{A.3}$$

where K_{wi} and θ_{ij} can be calculated by Eqs. (A.4) and (A.5).

$$K_{w_i} = \frac{B1_i\, T^{B2_i}}{1 + \frac{B3_i}{T} + \frac{B4_i}{T^2}} \tag{A.4}$$

$$\theta_{ij} = \frac{1}{4} \times \left[1 + \left[\left(\frac{\mu_i}{\mu_j}\right)\left(\frac{Mw_j}{Mw_i}\right)^{\frac{3}{4}}\left(\frac{T+S_i}{T+S_j}\right)\right]^{\frac{1}{2}}\right]^2 \times \frac{(T+S_{ij})}{(T+S_i)} \tag{A.5}$$

$$f_s = \begin{cases} 1 & nonpolar \\ 0.733 & polar \end{cases} \qquad S_{ij} = f_s\sqrt{S_i S_j} \qquad S_{iorj} = \begin{cases} 79 & for\ H_2\ only \\ 1.5 \times T_{B,i} & for\ other\ components \end{cases} \tag{A.6}$$

where B1, B2, B3 and B4 are constants which were provided by Lindsay and Bromley [65] and are presented in Table A.1.2.

Table A.1.2 – Constants for gas species corresponding to Eq. (A.4).

Component	B1	B2	B3	B4	T_B (K)
H_2	0.002653	0.7452	12	0	20.4
CO_2	3.69	−0.3838	964	1860000	194.7
CO	0.00059882	0.6863	57.13	501.92	81.7
CH_4	8.3983e-6	1.4268	−49.654	0	111.7
C_2H_4	8.6806e-6	1.4559	299.72	−29403	169.4
C_2H_6	0.000073869	1.1689	500.73	0	184.5
C_3H_6	0.0000449	1.2018	421	0	225.4
C_3H_8	−1.12	0.10972	−9834.6	−7535800	231.1
C_4H_8	0.000096809	1.1153	781.82	0	266.9
C_4H_{10}	0.051094	0.45253	5455.5	1979800	272.7
H_2O	6.2041e-6	1.3973	1.3973	0	373.2

Viscosity

The viscosity of the gas mixture, μ_g, can be calculated through Eq. (A.7).

$$\mu_g = \sum_{i=1}^{N} \frac{y_i \mu_{g,i}}{\sum_{j=1}^{N} y_j \sqrt{Mw_j/Mw_i}} \tag{A.7}$$

where $\mu_{g,i}$ is the viscosity of component "i" which can be estimated via the correlation proposed by Perry and Green in Eq. (A.8).

$$\mu_{g,i} = \frac{C1_i\, T^{C2_i}}{1 + C3_i + \frac{C4_i}{T^2}} \tag{A.8}$$

where C1, C2, C3 and C4 are constants which were provided in Perry and Green [64] and are presented in Table A.1.3.

Table A.1.3 – Constants for gas species corresponding to Eq. (A.8)

Component	C1	C2	C3	C4
H_2	1.79e-7	0.685	−0.59	140
CO	1.1127e-6	0.5338	94.7	0
CO_2	2.148e-6	0.46	290	0
CH_4	5.2546e-7	0.59006	105.67	0
C_2H_4	2.0789e-6	0.4163	352.7	0
C_2H_6	2.5906e-7	0.67988	98.902	0
C_3H_6	7.73919e-7	0.5423	263.73	0
C_3H_8	4.9054e-8	0.90125	0	0
C_4H_8	6.9744e-7	0.5462	305.25	0
C_4H_{10}	3.4387e-8	0.94604	0	0
H_2O	1.7096e-8	1.1146	0	0

A.2 Components molecular weights

Table A.2.1 – Molecular weights of components corresponding to Eqs. (A.5 and A.7).

Component	$Mw\left(\frac{g}{mol}\right)$
H_2	2.02
H_2O	18.02
CO	28.01
CO_2	44.01
CH_4	16.04
C_2H_4	28.054
C_2H_6	30.07
C_3H_8	44.096
C_3H_6	42.096
C_4H_8	56.123
C_4H_{10}	58.123

Appendix B

B.1 ABC Algorithm steps

1) Initialize the population of solutions X_{ij}, $i = 1,\ldots,SN$, $j = 1,\ldots,D$, where SN is the number of food sources, D is the dimension of the variables;
2) Compute the fitness values and evaluate the population;
3) Produce new solutions (food source positions) v_{ij} in the neighborhood of X_{ij} for the employed bees, using Eq. (B.1).

$$v_{ij,} = X_{ij} + \phi_{ij}(X_{ij} - X_{kj}) \tag{B.1}$$

where X_k is a randomly selected solution except X_i, ϕ_{ij} is a random number within the range $[-a, a]$, a is usually set up 1, then apply the greedy selection process between v_i and X_i;

4) Calculate the probability values p_i, for the solutions X_i by means of their fitness values fit_i, using Eq. (B.2):

$$p_i = fit_i \Big/ \left(\sum_{i=1}^{SN} fit_i\right) \tag{B.2}$$

where the fitness values might be calculated using Eq. (B.3) for minimization problems:

$$fit_i = \begin{cases} \frac{1}{1+f_i}, & if \quad f_i \geq 0 \\ 1 + abc(f_i), & if \quad f_i < 0 \end{cases} \tag{B.3}$$

where f_i is O.F value.

5) Produce new solutions (new positions) v_i, for the onlookers from the solutions X_i, selected depending on p_i, then apply the greedy selection process between v_i and X_i;
6) Determine the abandoned solution X_i, if exists, and replace it with a new randomly produced solution $X_{i,j}^{'}$ for the scout:

$$X_{ij,}^{'} = X\,min_j + rand(0,1) \times (X\,max_j - X\,min_j) \tag{B.4}$$

where $X\,min_j$ is the lower bound of the parameter j and $X\,max_j$ is the upper bound of the parameter j.

7) Memorize the best food source position (solution) achieved so far; if the stopping criteria is satisfied, then stop and output the best solution, otherwise go to step (2) and continue loop [66].

The values of kinetic parameters are determined via minimization of the O.F Eq (B.5).

$$O.F_{min} = {}^{1}/_{N} \sum_{j=1}^{D} (Desired\,output - Actual\,value)^2 \tag{B.5}$$

B.2 DE algorithm steps

Mutation

For each target vector $x_{i,G}$, a mutant vector is produced by

$$v_{i,G+1} = x_{i,G} + K \times (x_{r_1,G} - x_{i,G}) + F \times (x_{r_2,G} - x_{r_3,G}) \tag{B.6}$$

where $i, r_1, r_2, r_3 \in \{1, 2, ..., NP\}$ are randomly chosen and must be different from each other. In Eq. (B.6), F is the scaling factor which has an effect on the difference vector $(x_{r_2,G} - x_{r_3,G})$, K is the combination factor [53].

Crossover

The parent vector is mixed with the mutated vector to produce a trial vector $u_{ji,G+1}$

$$u_{ji,G+1} = \begin{cases} u_{ji,G+1} & if\,(md_j \leq CR)or\,j = rn_i, \\ q_{ji,G} & if\,(md_j \geq CR)and\,j \neq rn_i, \end{cases} \tag{B.7}$$

where $j = 1, 2, ..., D, rj \in [0, 1]$ is the random number, CR is crossover constant $\in [0, 1]$, and $rn_i \in (1, 2, ..., D)$ is the randomly chosen index [53].

Selection

All solutions in the population have the same chance of being selected as parents independent of their fitness values. The child produced after the mutation and crossover operations is evaluated. Then, the performance of the child vector is compared to that of parent and the better one is selected. If the parent is still better, it is retained in the population.

Fig. 4. a illustrates the steps of DE algorithm in detail: the difference between two population members (1, 2) is added to a third population member (3). The result (4) is subjected to crossover with the candidate for replacement (5) in order to obtain a proposal (6). The proposal is evaluated and replaces the candidate if it is found to be better.

REFERENCES

[1] Asif M, Gao X, Lv H, Xi X, Dong P. Catalytic hydrogenation of CO_2 from 600 MW supercritical coal power plant to produce methanol: a techno-economic analysis. Int J Hydrogen Energy 2018;43:2726–41.
[2] Atsonios K, Panopoulos KD, Kakaras E. Investigation of technical and economic aspects for methanol production through CO_2 hydrogenation. Int J Hydrogen Energy 2016;41:2202–14.
[3] De Falco M, Capocelli M, Basile A. Selective membrane application for the industrial one-step DME production process fed by CO_2 rich streams: modeling and simulation. Int J Hydrogen Energy 2017;42:6771–86.
[4] Gallucci F, Paturzo L, Basile A. An experimental study of CO_2 hydrogenation into methanol involving a zeolite membrane reactor. Chem Eng Process: Process Intensification 2004;43:1029–36.
[5] Voitic G, Pichler B, Basile A, Iulianelli A, Malli K, Bock S, et al. Chapter 10 - hydrogen production. In: Hacker V, Mitsushima S, editors. Fuel cells and hydrogen. Elsevier; 2018. p. 215–41.
[6] Nikoo MK, Saeidi S, Lohi A. A comparative thermodynamic analysis and experimental studies on hydrogen synthesis by supercritical water gasification of glucose. Clean Technol Environ Policy 2015;17:2267–88.
[7] Basile A, Campanari S, Manzolini G, Iulianelli A, Longo T, Liguori S, et al. Methane steam reforming in a Pd–Ag membrane reformer: an experimental study on reaction pressure influence at middle temperature. Int J Hydrogen Energy 2011;36:1531–9.
[8] Shahhosseini HR, Saeidi S, Najari S, Gallucci F. Comparison of conventional and spherical reactor for the industrial auto-thermal reforming of methane to maximize synthesis gas and minimize CO_2. Int J Hydrogen Energy 2017;42:19798–809.
[9] Wajda T, Gabriel K. Thermolysis reactor scale-up for pilot scale CuCl hybrid hydrogen production. Int J Hydrogen Energy 2018. https://doi.org/10.1016/j.ijhydene.2018.11.187.
[10] Basile A, Iulianelli A, Bagnato G, Dalena F. Hydrogen production for PEM fuel cells. In: Fang Z, Smith JRL, Qi X, editors. Production of hydrogen from renewable resources. Dordrecht: Springer Netherlands; 2015. p. 339–56.
[11] Acar C, Dincer I. Comparative assessment of hydrogen production methods from renewable and non-renewable sources. Int J Hydrogen Energy 2014;39:1–12.
[12] Vincenzo P, De falco M, Basile A. Sustainable development strategies: an overview. In: Vincenzo P, De falco M, Basile A, editors. Sustainable development in chemical engineering innovative technologies. John Wiley & Sons, Inc.; 2013. p. 1–24.
[13] Dincer I, Acar C. Innovation in hydrogen production. Int J Hydrogen Energy 2017;42:14843–64.
[14] Dincer I, Acar C. Smart energy solutions with hydrogen options. Int J Hydrogen Energy 2018;43:8579–99.
[15] Bičáková O, Straka P. Production of hydrogen from renewable resources and its effectiveness. Int J Hydrogen Energy 2012;37:11563–78.

[16] Saeidi S, Amin NAS, Rahimpour MR. Hydrogenation of CO_2 to value-added products—a review and potential future developments. J CO_2 utilization 2014;5:66–81.

[17] Cubeiro ML, Valderrama G, Goldwasser MR, González-Jiménez F, Da Silva MC, Pérez-Zurita MJ. Hydrogenation of CO and CO_2 with K and Mn promoted iron catalysts. In: de Pontes Rlecpnjhs M, Scurrell MS, editors. Studies in surface science and catalysis. Elsevier; 1997. p. 231–6.

[18] Jun K-W, Lee S-J, Kim H, Choi M-J, Lee K-W. Support effects of the promoted and unpromoted iron catalysts in CO_2 hydrogenation. In: Inui Makisy T, Yamaguchi T, editors. Studies in surface science and catalysis. Elsevier; 1998. p. 345–50.

[19] Weatherbee GD, Bartholomew CH. Hydrogenation of CO_2 on group VIII metals: IV. Specific activities and selectivities of silica-supported Co, Fe, and Ru. J Catal 1984;87:352–62.

[20] Willauer HD, Ananth R, Olsen MT, Drab DM, Hardy DR, Williams FW. Modeling and kinetic analysis of CO_2 hydrogenation using a Mn and K-promoted Fe catalyst in a fixed-bed reactor. J CO_2 Utilization 2013;3:56–64.

[21] Fiato RA, Iglesia E, Rice GW, Soled SL. Iron catalyzed CO_2 hydrogenation to liquid hydrocarbons. In: Inui MAKISY T, Yamaguchi T, editors. Studies in surface science and catalysis. Elsevier; 1998. p. 339–44.

[22] Tada S, Ikeda S, Shimoda N, Honma T, Takahashi M, Nariyuki A, et al. Sponge Ni catalyst with high activity in CO_2 methanation. Int J Hydrogen Energy 2017;42:30126–34.

[23] Bukhari SN, Chong CC, Teh LP, Vo D-VN, Ainirazali N, Triwahyono S, et al. Promising hydrothermal technique for efficient CO_2 methanation over Ni/SBA-15. Int J Hydrogen Energy 2018. https://doi.org/10.1016/j.ijhydene.2018.07.018.

[24] Spencer MS. On the activation energies of the forward and reverse water-gas shift reaction. Catal Lett 1995;32:9–13.

[25] Kaspar J, Graziani M, Rahman AM, Trovarelli A, Vichi EJS, da Silva EC. Carbon dioxide hydrogenation over iron containing catalysts. Appl Catal Gen 1994;117:125–37.

[26] Zhou R, Rui N, Fan Z, Liu C-j. Effect of the structure of Ni/TiO_2 catalyst on CO_2 methanation. Int J Hydrogen Energy 2016;41:22017–25.

[27] Riedel T, Schaub G, Jun K-W, Lee K-W. Kinetics of CO_2 hydrogenation on a K-promoted Fe catalyst. Ind Eng Chem Res 2001;40:1355–63.

[28] Saeidi S, Fazlollahi F, Najari S, Iranshahi D, Klemeš JJ, Baxter LL. Hydrogen production: perspectives, separation with special emphasis on kinetics of WGS reaction: a state-of-the-art review. J Ind Eng Chem 2017;49:1–25.

[29] De la Osa A, De Lucas A, Romero A, Valverde J, Sánchez P. Kinetic models discrimination for the high pressure WGS reaction over a commercial CoMo catalyst. Int J Hydrogen Energy 2011;36:9673–84.

[30] Schulz H, van Steen E, Claeys M. Specific inhibition as the kinetic principle of the Fischer-Tropsch synthesis. Top Catal 1995;2:223–34.

[31] Saeidi S, Amiri MT, Amin NAS, Rahimpour MR. Progress in reactors for high-temperature Fischer–Tropsch process: determination place of intensifier reactor perspective. Int J Chem React Eng 2014;12:1–26.

[32] Saeidi S, Nikoo MK, Mirvakili A, Bahrani S, Amin NAS, Rahimpour MR. Recent advances in reactors for low-temperature Fischer-Tropsch synthesis: process intensification perspective. Rev Chem Eng 2015;31:209–38.

[33] Lee M-D, Lee J-F, Chang C-S. Hydrogenation of carbon dioxide on unpromoted and potassium-promoted iron catalysts. Bull Chem Soc Jpn 1989;62:2756–8.

[34] Li W, Wang H, Jiang X, Zhu J, Liu Z, Guo X, et al. A short review of recent advances in CO_2 hydrogenation to hydrocarbons over heterogeneous catalysts. RSC Adv 2018;8:7651–69.

[35] Xie T, Wang J, Ding F, Zhang A, Li W, Guo X, et al. CO_2 hydrogenation to hydrocarbons over alumina-supported iron catalyst: effect of support pore size. J CO_2 Utilization 2017;19:202–8.

[36] Choi PH, Jun K-W, Lee S-J, Choi M-J, Lee K-W. Hydrogenation of carbon dioxide over alumina supported Fe-K catalysts. Catal Lett 1996;40:115–8.

[37] Ding F, Zhang A, Liu M, Guo X, Song C. Effect of SiO_2-coating of FeK/Al_2O_3 catalysts on their activity and selectivity for CO_2 hydrogenation to hydrocarbons. RSC Adv 2014;4:8930–8.

[38] Saeidi S, Najari S, Fazlollahi F, Nikoo MK, Sefidkon F, Klemeš JJ, et al. Mechanisms and kinetics of CO_2 hydrogenation to value-added products: a detailed review on current status and future trends. Renew Sustain Energy Rev 2017;80:1292–311.

[39] Lee S-C, Jang J-H, Lee B-Y, Kang M-C, Kang M, Choung S-J. The effect of binders on structure and chemical properties of Fe-K/γ-Al_2O_3 catalysts for CO_2 hydrogenation. Appl Catal Gen 2003;253:293–304.

[40] Choudhary V, Devadas P, Kinage A, Guisnet M. Influence of binder on the acidity and performance of H-Gallosilicate (MFI) zeolite in propane aromatization. Appl Catal Gen 1997;162:223–33.

[41] Willauer HD, Ananth R, Olsen MT, Drab DM, Hardy DR, Williams FW. Modeling and kinetic analysis of CO_2 hydrogenation using a Mn and K-promoted Fe catalyst in a fixed-bed reactor. J CO_2 Utilization 2013;3–4:56–64.

[42] Yan X, Chen D, Hu S, Ding J. Estimation of kinetic parameters using chaos genetic algorithms. J Chemical Industry and Eng-China 2002;53:810–4.

[43] Chen G, Wang J, Li R. Identification of parameters in chemical kinetics using a hybrid algorithm of artificial bee colony algorithm and simplex. Artificial Intelligence and Computational Intelligence. Springer; 2011. p. 220–7.

[44] Hu C, Yan X. A novel adaptive differential evolution algorithm with application to estimate kinetic parameters of oxidation in supercritical water. Eng Optim 2009;41:1051–62.

[45] Chen G, Wang J, Li C. Identification of parameters in kinetic models using artificial bee colony algorithm. Berlin, Heidelberg: Springer Berlin Heidelberg; 2012. p. 323–9.

[46] Lin H-Y, Chen Y-W, Li C. The mechanism of reduction of iron oxide by hydrogen. Thermochim Acta 2003;400:61–7.

[47] Ghouse JH, Adams TA. A multi-scale dynamic two-dimensional heterogeneous model for catalytic steam methane reforming reactors. Int J Hydrogen Energy 2013;38:9984–99.

[48] Adams TA, Barton PI. A dynamic two-dimensional heterogeneous model for water gas shift reactors. Int J Hydrogen Energy 2009;34:8877–91.

[49] Rohde MP, Unruh D, Schaub G. Membrane application in Fischer–Tropsch synthesis to enhance CO_2 hydrogenation. Ind Eng Chem Res 2005;44:9653–8.

[50] Astudillo L, Melin P, Castillo O. Introduction to an optimization algorithm based on the chemical reactions. Inf Sci 2015;291:85–95.

[51] Karaboga D. Artificial bee colony algorithm. Scholarpedia 2010;5:6915.

[52] Iranshahi D, Hamedi N, Nategh M, Saeedi R, Saeidi S. Thermal integration of sulfuric acid and continuous catalyst regeneration of naphtha reforming plants. Chem Eng Technol 2018;41:637–55.

[53] Storn R, Price K. Differential evolution – a simple and efficient heuristic for global optimization over continuous spaces. J Global Optim 1997;11:341–59.

[54] Rahimpour MR, Parvasi P, Setoodeh P. Dynamic optimization of a novel radial-flow, spherical-bed methanol synthesis reactor in the presence of catalyst deactivation using Differential Evolution (DE) algorithm. Int J Hydrogen Energy 2009;34:6221–30.

[55] Choi M-J, Kim J-S, Kim H-K, Lee S-B, Kang Y, Lee K-W. Hydrogenation of CO_2 over Fe-K based catalysts in a fixed bed reactors at elevated pressure. Kor J Chem Eng 2001;18:646–51.
[56] Kim J-S, Lee S, Lee S-B, Choi M-J, Lee K-W. Performance of catalytic reactors for the hydrogenation of CO_2 to hydrocarbons. Catal Today 2006;115:228–34.
[57] Lee S-B, Kim J-S, Lee W-Y, Lee K-W, Choi M-J. Product distribution analysis for catalytic reduction of CO_2 in a bench scale fixed bed reactor. In: Park S-E, Chang J-S, Lee K-W, editors. Studies in surface science and catalysis. Elsevier; 2004. p. 73–8.
[58] Riedel T, Claeys M, Schulz H, Schaub G, Nam S-S, Jun K-W, et al. Comparative study of Fischer–Tropsch synthesis with H_2/CO and H_2/CO_2 syngas using Fe- and Co-based catalysts. Appl Catal Gen 1999;186:201–13.
[59] OR E, Davide M, Pawel P, JM D. Kinetics of CO_2 hydrogenation to hydrocarbons over iron–silica catalysts. ChemPhysChem 2017;18:3211–8.
[60] Visconti CG, Martinelli M, Falbo L, Infantes-Molina A, Lietti L, Forzatti P, et al. CO_2 hydrogenation to lower olefins on a high surface area K-promoted bulk Fe-catalyst. Appl Catal B Environ 2017;200:530–42.
[61] Ding F, Zhang A, Liu M, Zuo Y, Li K, Guo X, et al. CO_2 hydrogenation to hydrocarbons over iron-based catalyst: effects of physicochemical properties of Al_2O_3 supports. Ind Eng Chem Res 2014;53:17563–9.
[62] Satthawong R, Koizumi N, Song C, Prasassarakich P. Comparative study on CO_2 hydrogenation to higher hydrocarbons over Fe-based bimetallic catalysts. Top Catal 2014;57:588–94.
[63] Wang W, Jiang X, Wang X, Song C. Fe–Cu bimetallic catalysts for selective CO_2 hydrogenation to olefin-rich C_2^+ hydrocarbons. Ind Eng Chem Res 2018;57:4535–42.
[64] Green DW, Perry RH. Perry's chemical engineers' handbook. In: Don W, Green y, Perry Robert H, editors; 1973.
[65] Lindsay AL, Bromley LA. Thermal conductivity of gas mixtures. Ind Eng Chem 1950;42:1508–11.
[66] Karaboga D, Basturk B. On the performance of artificial bee colony (ABC) algorithm. Appl Soft Comput 2008;8:687–97.